國立交通大學

材料科學與工程學系

博士論文

以 PS-b-PEO 與 PS-b-P4VP 塊式高分子操控 CdS 奈米粒子形成二維與三維奈米陣列並探討其對於塊式高分子型態之影響

Fabrications of 2-D and 3-D CdS Arrays by PS-b-PEO and PS-b-P4VP Templates and Effects of CdS on the Morphological Transformation of Block Copolymers

研究生： 葉孝蔚 **(Siao-Wei Yeh)**

指導教授： 韋光華 **(Kung-Hwa Wei)**

中華民國 九十四年 一月

Abstract

In this thesis, 3-D nanostructure of CdS clusters by dispersing pre-synthesized CdS nanoparticles, containing hydroxyl groups on surface, in the PEO block selectively of polystyrene-b-poly(ethylene oxide) (SEO) block copolymers as template in the bulk form was prepared, and the effects of surface-modified CdS nanoparticles on the crystallinity and morphological transformation of bulk SEO block copolymers were discussed in Chapter 2. In the **Amorphous-Crystalline Bulk SEO** system, CdS nanoparticles hinder crystallization of PEO domains, and induce the composites form a structure decided by the volume fraction only. (**BCC** structure for $\mathbf{V_{PEO/HSEO} = 0.11}$**, and HEX structure for** $\mathbf{V_{PEO/LSEO} = 0.39}$)

The effects of hydrogen bonding between surface-hydroxylated CdS clusters and PEO chains on morphological transformation of the CdS/SEO thin film were illustrated in Chapter 3. Ordered 2-D spatial arrangement of CdS clusters in monolayered SEO thin films by using solvent selectivity to sequester CdS nanoparticles in PEO domains of SEO block copolymer thin films was fabricated. Large-scale ordered structure of CdS clusters is available by a patterned substrate. Surface-modified CdS nanoparticles maintain their original optical properties.

Moreover, the morphological transformation of polystyrene-b-poly(4-vinylpyridine) (S4VP) to a lamellar structure from a cylindrical structure by incorporating CdS nanoparticles were also demonstrated in Chapter 4. CdS nanoparticles, in this case, containing a chemically-active carboxylic acid groups on surface were modified by mercaptoacetic acid and connected to the pyridine groups in the poly(4-vinylpyridine) (P4VP) chains of S4VP block copolymers. This morphological transformation, induced by hydrogen bonding between CdS nanoparticles and P4VP chains, is consistent with the phase diagram predicted by a theoretical study of the copolymer/particle mixture system.

We can concluded that the final structure of nanoparticles/bloc copolymers system is also affected by the interaction parameter. The interaction parameter between the two phases in nanoparticles/block copolymers system is related to the intermolecular force between nanoparticles and block copolymers, such as the formation and reduction of hydrogen bonds and crystallization.

摘要

此論文主旨為利用有機雙塊式高分子自身組織成二維與三維週期性結構的特性作為模版，操控無機 CdS 奈米粒子，形成特定結構之奈米陣列，並探討 CdS 奈米粒子對塊式高分子結構造成之影響。

在第二章中，利用不同分子量之 PS-b-PEO 塊式高分子操控 CdS 奈米粒子形成體心立方(body-center cubic)與六方柱狀(hexagonal-packed cylinders)結構之奈米複材，並探討 CdS 奈米粒子表面之-OH 基對於塊式高分子微結構之影響。CdS 奈米粒子破壞 PEO domains 的結晶特性導致在 amorphous-crystalline PS-b-PEO 中的奈米複材之最後結構將僅取決於其體積分率。

在第三章中，以不同分子量之 PS-b-PEO 塊式高分子操控 CdS 奈米粒子製備形成二維特殊結構 CdS 陣列，並探討 CdS 奈米粒子表面之-OH 基對於塊式高分子薄膜結構從柱狀結構至球狀結構之轉換。 可利用分子量來操控 CdS 奈米團的間隔，並可以利用 patterned substrate 來達到大面積的規則結構。 CdS 奈米粒子的光學特性並不會因為塊式高分子操控的影響改變其原本光學特性。

第四章中則利用 PS-b-P4VP 塊式高分子操控 CdS 奈米粒子形成層狀結構之奈米複材，並探討 CdS 表面-COOH 基對於塊式高分子結構從柱狀結構至層狀結構之轉換。此種奈米結構轉換結果與文獻中理論推導的計算結果相符合。

我們藉由本論文的研究結果可以得到以下結論，利用奈米粒子與對於塊式高分子之間所造成的分子間作用引力(結晶形成與破壞、形成氫鍵之強弱)，將會影響塊式高分子兩項間的引力參數(interaction parameter)，進而影響奈米複材最後之結構與特性。

誌謝

論文口試結束後，開車回家的路上，七年來在實驗室的點滴，投影片般浮現在腦海裡。

從大學四年級剛進實驗室的專題研究到博士論文的口試完成，萬分感謝指導教授韋光華老師的指導，使我在人格特質與專業能力上都有顯著的成長。

感謝我的口試委員梁耕三老師、鄭有舜博士、邱文英老師、黃華宗老師、林宏洲老師，在您們的指導下，讓我獲益良多，真的感謝！！

在論文的研究過程中，尤其要感謝同步輻射中心梁耕三老師、鄭有舜博士、孫亞賢博士、賴英煌博士與學妹的男友品鈞學長在實驗研究與討論上的協助，也讓我學習到嚴謹的態度及深入的探討是作研究的必備條件。

在研究生生涯的學長、學姐們，充哥、小田學長、田帥帥、良祐、米奇、小豬等學長們，在這段時間的教導與鼓勵，讓我克服了萬難往前的衝、衝、衝。蔡欣瑩學姐不時的牛肉麵午餐邀約，讓我在實驗彈性疲乏之餘，可以藉牛肉的香味及好喝的湯頭讓我精神百倍。

另外感謝實驗室曾經在我研究生生涯出現過的大大小小，蕭家傑學長、吳昭瑩學姐，振道與岱慶的酒量、已婚的麗娟阿姐仔的麻辣鍋與芒果青、房子在竹北的汪信亨、令人難忘的巫真瑋、雙胞胎的老爸兼實驗室亂源 apo、龜龜的阿標、善良愛哭又不聯絡的沈妙玲、在工研院放火的鄭欽峰、好心的老周跟耀德、聰明好心又不像處女座的琬琪、老師最疼的世莉、嘰哩刮啦又可愛又好心的克瑤、閱人無數的阿茂、阿茂的同學阿諄、無機三人組(學弟的女友靜怡、天才孟婷與麻棘手含章)、學妹的男友機車大饅頭、牛一般的國峰、遠在中研院的小玫、其實蠻愛講話也是天蠍座的許公子、實驗室明日之星邱茂源與王旭生、要直升又成績不好的陳振平、搬家用的李紹睿，還有三位印度籍洋將 Reddy, Kens and 好心又認真的 Dina，都讓人印象深刻。　另外，隔壁實驗室的趙老大、美蕙學姐、”龜中之王”小賢、學長的女友佩君學姐、香味十足的南哥、在德國打拼的守謙、台積電的淑慧、有前途的帥哥阿家、在旺宏的虎爛王黃俊清……，也感謝他們在這過程中的參與。

最最最最最最感謝的是遠在高雄的爹娘，感謝您們的包容與支持鼓勵，太感謝了！！！ 還有所有的親友們，岳父、岳母，愛犬小雷，感謝感謝！！

我親愛的老婆，天鳳，感謝你這幾年來的犧牲、包容與支持，有妳真好！！還有我的貓咪，gugi，在我弄 paper 很累時，看到妳心情就變好了。

還有關心我的朋友們、赤兔隊友與球友們，謝謝大家！！

Table of Content

Figure Lists

Chapter 1: Introduction

Chapter 2: Effects of CdS in SEO bulk samples

Scheme & Table Lists

Chapter 1: Introduction

Chapter 2: Effects of CdS in SEO bulk samples

Chapter 3: Effects of CdS in SEO thin films

Chapter 4: Effects of CdS in S4VP bulk samples

Chapter 1: Introduction

1-1 Block copolymers

Block copolymers are composed of long sequences ("blocks") of the same monomer unit, covalently bound to sequences of unlike type. The blocks can be connected in a variety of ways; schematics of AB diblock and ABA triblock structures are shown in Figure 1-1-1.

Block copolymers exhibit microphase separation of the dissimilar blocks and self-assemble to a specific 2-D or 3-D structure in a nanometer scale.[1] For example, depending upon the relative block volume fraction, spheres, cylinders, or lamellae of PS in a PB matrix are possible. More recently, a bicontinuous morphology has been observed in PS-polyisoprene (PI) block copolymers. This newly discovered morphology has been coined the ordered bicontinuous double diamond (OBDD). This bicontinuous structure in PS-PI star block copolymers with PI as the major component has been observed.[2] Similarly, Hasegawa and coworkers have observed the inverse of OBDD in the linear block copolymers with PS as the major component. Figure 1-1-2 shows the range of microstrucures possible in PS-PI block copolymers. However, these morphologies are considered as applying to PS-PI block copolymer systems.

The morphology will affect the bulk properties of BCP. The properties affected include the mechanical strength and toughness of the polymer as well as the gas permeation properties. For instance, Thomas and coworkers have conducted gas diffusion and solubility studies on various Kraton PS-PB block copolymers, materials exhibiting a variety of morphologies. Models of diffusion and the solubility of gases in the polymers developed by Sax and Ottino were used to predict the diffusional

properties of the carbon dioxide in various membranes. These rather simple models were successful for the various phase separated morphologies investigated, such as body centered cubic spheres, hexagonally packed cylinders, lamellae, and OBDD. These studies show that the gas transport properties are influenced, not only by the volume fraction of the respective blocks, but also by the morphology and connectivity of different phases.

On the other hand, block copolymers in the solution state, like low molecular weight surfactants, form micelles in solvents selective for one of the blocks. Tuzar reported the insoluble block forms the core of such structures, whereas the soluble block forms the corona. The phenomenon of micellization has been studied for many decades by Hamley et al., both from theoretical as well as from the experimental points of view, due to the potential applications of micellar systems in areas like viscosity modification of fluids, cosmetics, pharmacy, lubrication of surfaces, emulsification, solubilization of insoluble substances, drug delivery and environmental purification methodologies in Tuzar, Haulbrook and Harada groups.

Two of the main questions that predominate in the study of micelle formation by block copolymers are the question of the structure of an isolated micelle and the question of the configuration of a block copolymer chain incorporated in a micelle. Complications arising from the presence of unimers (unassociated copolymer chains), possible long-range ordering of the micelles, intermicellar interactions, etc. should be considered. The generally accepted idea is that most block copolymer micelles are spherical with a relatively compact core consisting of the insoluble blocks and a corona consisting of the soluble ones. The chains in the core can be considered to be in a state resembling the homopolymer melt if the solvent is very poor for them (i.e., highly selective). Tuzar et al. reported that some swelling of the core by solvent molecules cannot be ruled out, especially in cases of low selectivity. The corona is

formed by the soluble blocks, which are in a well-solvated state but considerably stretched because of geometrical constrains, especially in the region near the core. Cylindrical micelles have also been observed in several cases by Nakano, Mortensen, Schillen, Zhao and Ding. This change in the overall structure may be due to the high content of the block copolymer in the insoluble part, to the block copolymer architecture, and also to the selectivity of the solvent. Clusters of micelles have been identified in Moffit's and Zhang's groups.

Applications

Conventional and potential high-technology applications of block copolymers are based on their ability to self-assemble, in bulk or in selective solvents, into ordered nanostructures, with dimensions comparable to chain dimensions.[3] By changing the molecular weight, chemical structure, molecular architecture, and composition of block copolymers, the size scale, the type of ordering, and the characteristics of these nanostructures can be manipulated.

Several potential high-technology applications of block copolymers are based on their ability to self-assemble, in bulk or in selective solvents, into ordered nanostructures. Block copolymers, when dissolved in liquids that are solvents for one block but nonsolvents for the other (i.e., selective solvents), self-associate usually in spherical micelles of nearly uniform size. The insoluble blocks form the core and the soluble blocks the shell of the micelles. This phenomenon can be used for encapsulation and selective delivery or removal of organic/inorganic compounds.

Due to the miniaturization of electronic, optoelectronic, and magnetic devices, nanometer-scale patterning of materials is an important objective of current science and technology. Block copolymers, which have the ability to self-assemble into periodic ordered microstructures, are recognized to be promising candidates for patterning nanostructures. By changing the molecular weight, chemical nature,

molecular architecture, and composition of the copolymer, one can control the size and type of ordering. A few examples of nanopatterning by using block copolymers are presented in the following text.

Nanopatterning is very important for lithography. Nanosizes greater than 150 nm can be routinely produced by photolithography techniques. The minimum size that can be achieved by photolithography is determined by the wavelength of light used in the exposure. Electron beam lithography is commonly used to access feature sizes between 150 nm and 30 nm. However, sizes less than 30 nm are not easily obtained by standard lithography. One way to overcome this problem is by using self-assembled block copolymers. Dense, periodic arrays of holes and dots have been fabricated on a silicon nitride-coated silicon wafer using block copolymers of styrene and butadiene, polystyrene-b-polybutadiene by Park's and Harrison's groups. By using the same principle, various dense nanometer patterns can be produced using block copolymers. For example, parallel lines can be produced either by a film of lamellae, which are oriented normal to the substrate or of cylinders that lie parallel to the surface. Diblock copolymers of styrene and methylmethacrylate were used to produce templates for dense nanowire arrays by Thurn-Albrecht et al. The pores can be also filled with silicon tetrachloride, and, by hydrolysis with traces of water (nanoreactor), an array of silicon oxide posts in an organic matrix is produced by Kim et al.

By using block copolymers, nanoporous and nanorelief ceramic films can be prepared with important applications as selective separation membranes, next generation catalysts, and photonic materials. The ceramic network structure derived from PI-DG copolymer has potential use in interconnects because of its low dielectric constant, high-temperature stability, and the inherent etch selectivity of this material to photoresist. These periodic and interconnected high dielectric/low dielectric

ceramic/air structures also have potential as photonic band gap materials

1-2 Nanoparticles

Nanoparticles play an important role for nanotechnology and livelihood applications, for example catalysts, light-emitting diode, etc. Recently, many kinds of metal, metal oxide or semiconductor nanoparticles were reported for applications, such as Au or CdSe nanoparticles for bio-labeling and solar devices, TiO_2 nanoparticles for photo-catalysis materials, Co, $CoFe_2O_4$ and Fe_2O_3 nanoparticles for magnetic applications. For semiconductor nanoparticles with sizes close to their Bohr exciton radius (typically between 1-10 nm), the size-dependent band gap results in tunable optical properties. These semiconductor nanoparticles are termed as quantum dots because their tunable optical properties can be predicted by quantum mechanics. Among these studies, quantum confined semiconductor nanoparticles, such as CdS and CdSe/ZnS, are highly potential to light emitting diode devices.

1-3 The reason for the research

The interaction between surface-modified nanoparticles and the block copolymer chains to affect the crystallinity and morphology of the block copolymer bulk samples and thin films is interesting. On the part of block copolymers in bulk form, the selective dispersion of pre-synthesized inorganic nanoparticles in one domain of a block copolymer and the fabrication of 3-D inorganic nanostructures by the block copolymer template improve the potential for optical applications, due to specific properties of nanoparticles and the increase of the refractive index contrast between phase-separated periodic domains of block copolymers. On the other hands, by block copolymer thin films as template, the ordered 2-D inorganic clusters

arrangement is important for several applications, such as nanomasks for lithography, nanotemplates for growing nanostructures, and devices.

1-4 Materials

In this thesis, asymmetric polystyrene-b-poly(ethylene oxide) (SEO) and poly(styrene-b-4-vinylpyridine) (S4VP) are used for this research due to various structures in amorphous-crystalline diblock copolymers and CdS nanoparticles are chosen because of their inherently interesting electronic and photophysical properties.

For the present study, two asymmetric polystyrene-b-poly(ethylene oxide) diblock copolymers (SEO), having a higher molecular weight (MW) (MW_{PS}/MW_{PEO} = 125k/16.1k) termed HSEO, and a lower MW (Mw_{PS}/Mw_{PEO} = 19k/12.6k) termed LSEO, were used. The volume fraction of PEO in HSEO is 0.11 and that in LSEO is 0.39. Poly(styrene-b-4-vinylpyridine) (S4VP) diblock copolymer with a molecular weight of 47.6kPS/20.9kP4VP (the volume fraction of P4VP domains being 0.3) was used. These block copolymers, with polydispersion index (PDI) < 1.1, were purchased from Polymersource Inc.

Two kinds of CdS nanoparticles were synthesized with mercaptoethanol and mercaptoacetic acid as the surfactant by reacting cadmium acetate dehydrate ($Cd(Ac)_2 \cdot 2H_2O$), sodium sulfide (Na_2S), mercaptoethanol (HSC_2H_4OH) in methanol, following a modification of the kinetic trapping method.[4b,4c] After filtration, CdS QDs were collected and then dispersed in N, N-dimethylforamide (DMF). In our case, surfactant-modified CdS containing a chemically active hydroxyl and carboxylic acid groups on surface, as shown in Scheme 1-1, become hydrophilic, and their basic properties are given in Table 1-1. In Table 1-1, The average size of the surface-modified CdS nanoparticles in DMF can be characterized by the Schultz

distribution of a mean radius of 18.4 Å and a polydispersity of 0.5, as shown in Figure 1-4-1.[5] Figure 1-4-1 shows the SAXS data for the CdS solution in DMF. The data can be simulated reasonably well (dashed curve) using a spherical shape and the Schultz size distribution shown in the inset. The two key parameters of the size distribution obtained from the fitting process are the mean radius r_a = 18.4 Å and the polydispersity p = 0.5. The most probable radius, r_p, calculated is 9.6 Å. To reduce fitting parameters, we have fitted the data to in an absolute scattering intensity scale, using the CdS concentration 0.035 wt. %, and a scattering-length density (SLD) of 8.78×10^{-6} Å^{-2} for DMF while 49.85×10^{-6} Å^{-2} for CdS nanoparticles of a density of 6.63 g/cm^3. The density for CdS is estimated from the X-ray diffraction data for the CdS powder.

The size distribution of CdS is calculated from the UV-Vis spectrum of CdS in DMF in Figure 1-4-2(a). Moreover, the CdS size obtained from the X-ray diffraction in Figure 1-4-2(b) is the crystal size, which is the smallest and corresponds to the fact that we have poly-crystal CdS. Figure 1-4-2(a) shows UV-vis absorption and photoluminescence spectra of the CdS nanoparticles. In the UV-Vis absorption spectrum, a blue shift (68 nm) in the absorption edge (447nm) with respect to the bulk value (515 nm) and the appearance of an exciton shoulder and a blue-shift of the absorption edge indicate that the CdS nanoparticles are quantum-confined.[4a,4d] From the absorption wavelength, the size of the CdS nanoparticles can be calculated using equation (1).

$$Eg_{abs} - Eg_{ref} = \Delta Eg \approx \frac{\hbar^2\pi^2}{2R^2}\bullet\frac{1}{\mu} - \frac{1.8e^2}{\varepsilon R} \qquad (1)$$

Here, R is the radius of the particle, μ is the reduced mass of the exciton, i.e., $\mu^{-1} = m_h^{*-1} + m_e^{*-1}$, where m^*_e is the effective mass of the electron, m^*_h is the effective mass of the hole and ε is the dielectric constant of the material. From UV-vis

absorption spectrum, two CdS sizes (3.4 nm for $2R_{edge}$ and 2.0 nm for $2R_{\max}$), as listed in Table 1-1, are calculated individually from edge absorption wavelength λ_{edge} and $\lambda_{\max}$. The λ_{edge} and $\lambda_{\max}$ correspond to the larger mean particles size and the mode size in a size distribution, respectively. The sizes of CdS in DMF, determined by energy gaps of semiconductors from UV-vis absorption spectra, are consistent with that calculated by small-angle X-ray scattering in an absolute intensity scale in previous studies. The polydispersity of the sample is assessed by calculating the half-width of size distribution ($d_{1/2}$), 1.4nm, defined as

$$d_{1/2} = 2R_{edge} - 2R_{\max} \qquad (2)$$

If we assume a Gaussian distribution of particles, $d_{1/2}$ value can be taken to be twice of that of the standard deviation (σ_{2R}), and $2R_{\max}$ approximate the mean particle diameter ($2R_{mean}$). Then, a simplified radius polydispersity index (RPI) can be defined in equation (3).

$$RPI = \left(\sigma_{2R} / 2R_{mean}\right)^2 + 1 \qquad (3)$$

As shown in Table 1-1, RPI for the CdS nanoparticles in this case is about 1.12.

The photoluminescence of CdS in DMF, as shown in Figure 1-4-2(a), exhibits a sharp excitonic fluorescence at 478 nm and two broad peaks at 683 nm and 717 nm, which are due to two different states of surface-trapping.[4d] The fluorescence by surface trapped states, which exhibited by most nanoparticles, results from a nonradiative decay of the free electrons to the deep-trapped state; it does not indicate a highly agglomeration of CdS nanoparticles. In the present study, the intensity of surface-trapped fluorescence is much stronger than that of the excitonic fluorescence, indicating a poor passivation of the surface state of CdS nanoparticles. This could be caused by the defects of CdS nanocrystals or the surface modification by

mercaptoethanol.[4a,4d]

Figure 1-4-2(b) shows X-ray diffraction curves of the CdS powders, which have broad peaks (2θ = 20°~40°) associated with their sphalerite structure. In the case of spherical crystallites, the relation between L, the coherence length, and *D* (diameter of CdS) is given by *L*=3/4*D*. *L* is calculated from the Debye-Scherrer formula, given by equation (4).

$$L = \frac{0.9\lambda}{B\cos\theta} \qquad (4)$$

where *B* is the full width at half maximum of the peak, λ is the X-ray wavelength, and θ is the angle of diffraction. The crystal size of CdS determined by this method is 1.33 nm. It should be noted that the CdS size obtained from X-ray diffraction is the crystal size, and represents the smallest size, corresponding to the fact that we have polycrystalline CdS.

Reference

1. Bates, F.S. Washington Science 1991, 251, 898.

2. Herman, D.S.; Kinning, D.J.; Thomas, E.L.; Fetters, L.J. Macromolecules 1987, 20, 2940.

3. Hadjichristidis, N.; Pispas, S.; Floudas, G. "Block CopolymersSynthetic Strategies, Physical Properties, and Applications"

4. a) Henglein, A. Chem. Rev. 1989, 89, 1861. (b) Veinot, J. G. C.; Ginzburg, M.; Pietro, W. J. Chem. Mater. 1997, 9, 2117. (c) Herron, N.; Wang, Y.; Eckert, H. J. Am. Chem. Soc. 1990, 112, 1322. (d) Brus, L. J. Phys. Chem. 1986, 90, 2555.

5. U-Ser Jeng, Ya-Sen Sun, Hsin-Yi Lee, Chia-Hung Hsu, and Keng S. Liang, Siao-Wei Yeh, Kung-Hwa Wei, *Macromolecules* **2004**, *37*, 4617.

Scheme 1-1 Synthesis of surface-modified CdS nanoparticles by mercaptoethanol and mercaptoacetic acid

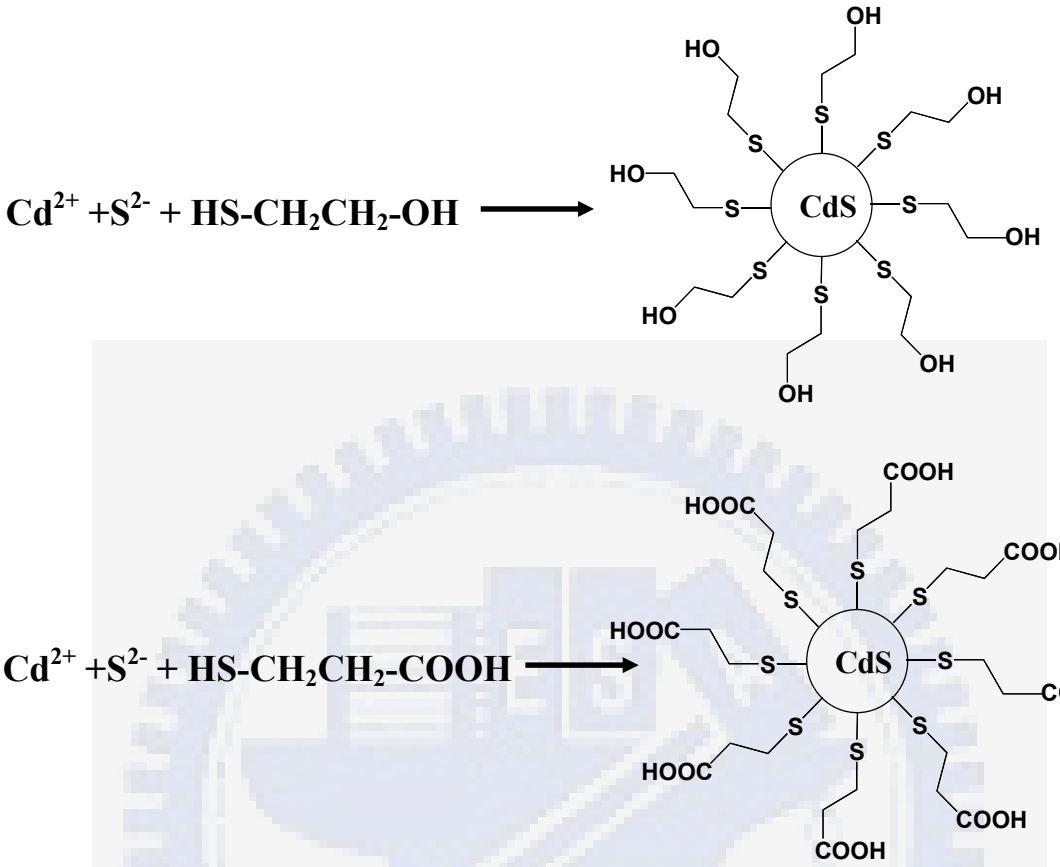

Table 1-1: Characteristic properties of CdS nanoparticles

λ_{edge} [a]	λ_{max} [b]	$2R_{edge}$ [c]	$2R_{max}$ [d]	RPI [e]	Crystal size[f]	Average particle size[g]
445 nm	360 nm	3.4 nm	2.0 nm	1.12	1.33 nm	3.6 nm

[a] The edge absorption wavelength of CdS nanoparticles in DMF as obtained from UV-vis spectra in Figure 1-4-2(a).

[b] The absorption wavelength of the mode of CdS nanoparticles.

[c] The larger size of CdS nanoparticles were calculated with λ_{edge} by UV-vis spectra using equation (1).[4a,4d]

[d]. The mode of the CdS size was calculated from λ_{max} .

[e] The radius dispersity index (RPI) were determined by equation (3).

[f] Crystal sizes are calculated using the Debye-Scherrer equation.

[g] The averaged size of CdS was obtained from SAXS curves of CdS in DMF in Figure 1-4-1.

Figure Captions

Figure 1-1-1. Schematics of AB diblock and ABA triblock copolymers structures

Figure 1-1-2. Possible phase separated morphologies in PD-PS block copolymer systems. f_A refers to the volume fraction of the A block, which in this case is polystyrene.

Figure 1-1-3. Typical nanostructures indicating the LAM: lamellar, HCPC: hexagonally packed cylinders, PC: primitive or simple cubic, BCC: body-centered cubic, FCC: face-centered cubic, HCPS: hexagonally closed packed spheres, DD: double diamond, Ia_3d and Pm_3n (adapted from Burger 2002).

Figure 1-4-1. SAXS data for the DMF solution of 0.035 wt. % CdS nanoparticles, fitted (dashed curve) using the Schultz size distribution with the mean radius r_a and polydispersity p values shown in the inset. The peak value r_p is the most-likely observed radius in the distribution. (U-Ser Jeng, Ya-Sen Sun, Hsin-Yi Lee, Chia-Hung Hsu, and Keng S. Liang, Siao-Wei Yeh, Kung-Hwa Wei, "The binding effect of surface-modified cadmium sulfide on the microstructure of PS-b-PEO block copolymers", *Macromolecules* **2004**, *37*, 4617.)

Figure 1-4-2. (a) UV-vis absorption and photoluminescence spectra of mercaptoethanol-modified CdS nanoparticles in N, N-dimethylforamide (DMF). (b) The X-ray diffraction curve of mercaptoethanol -modified CdS nanoparticles.

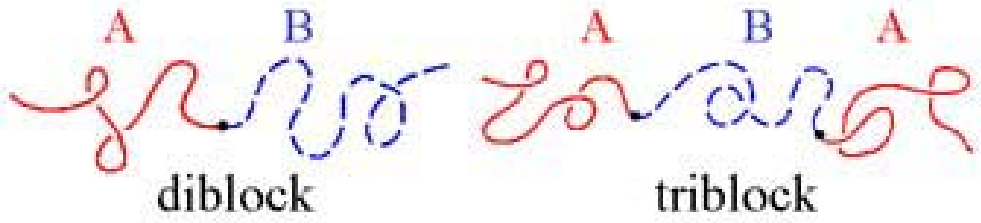

Figure 1-1-1

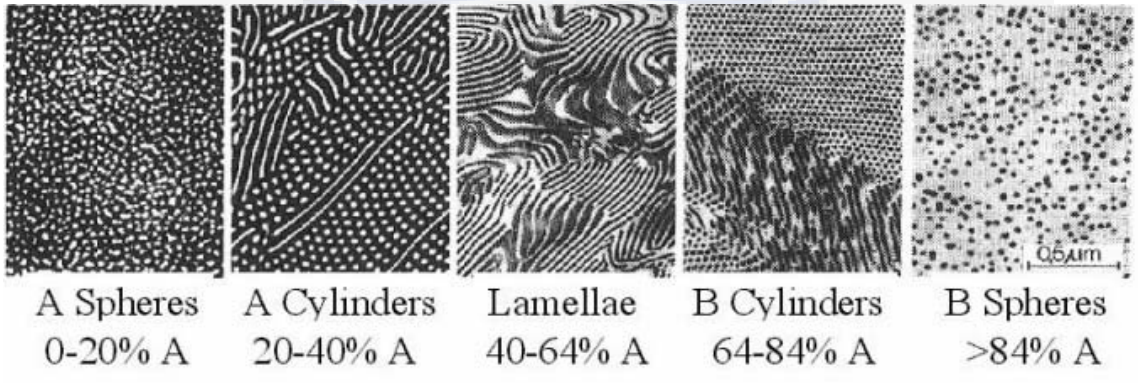

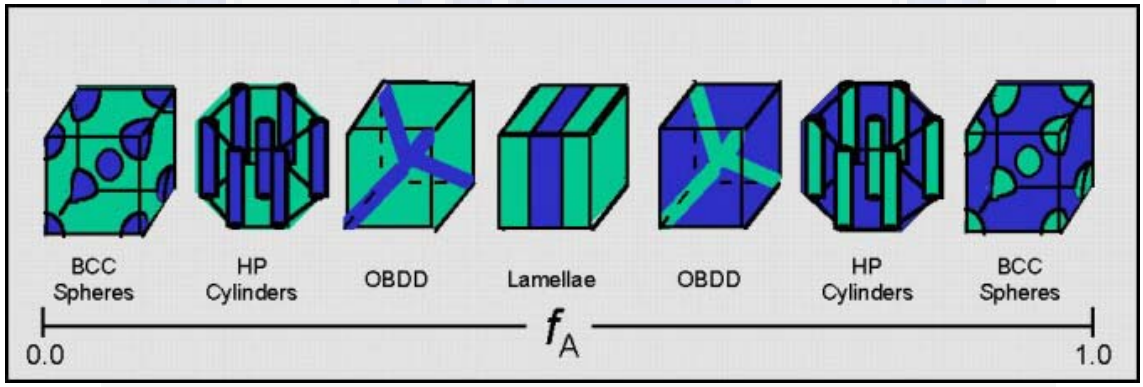

Figure 1-1-2

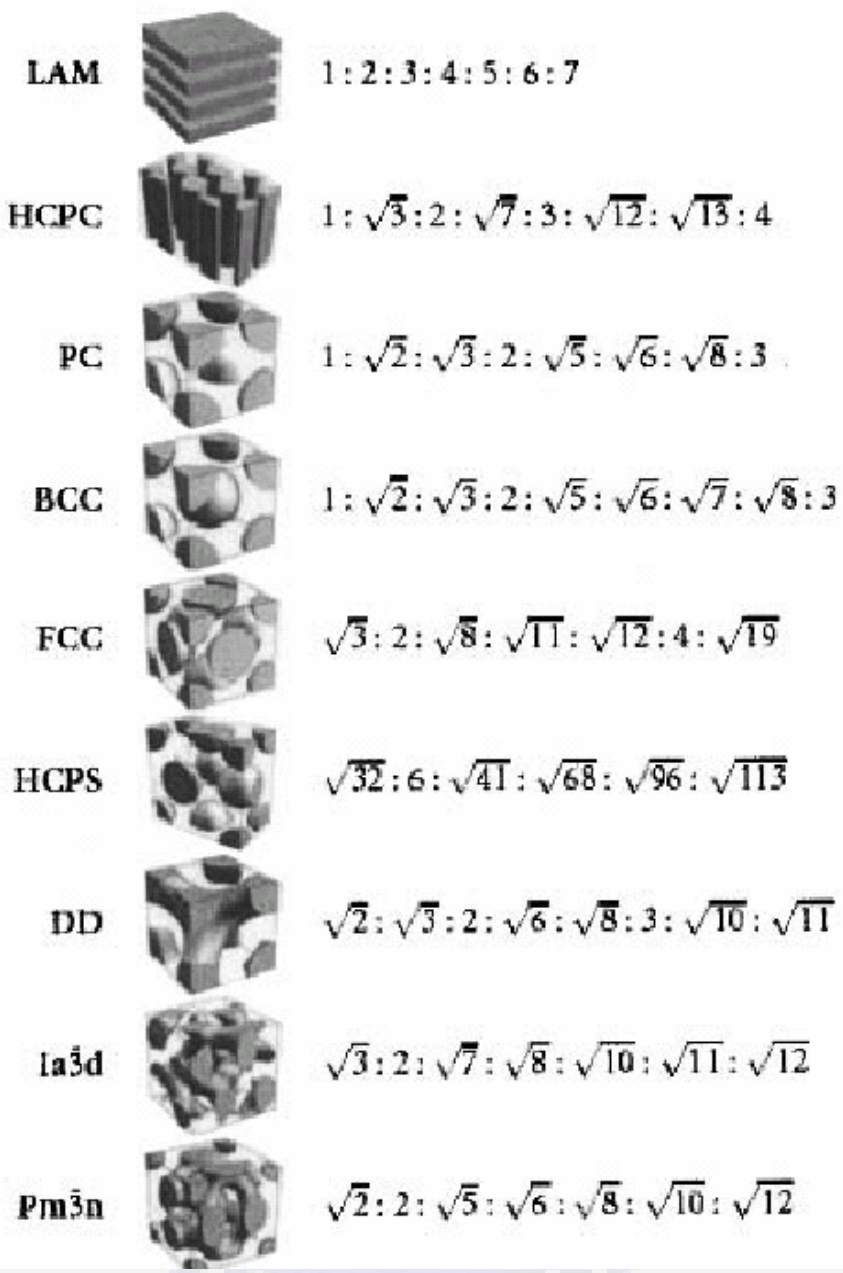
LAM
1 : 2 : 3 : 4 : 5 : 6 : 7
HCPC
1 : √3 : 2 : √7 : 3 : √12 : √13 : 4
PC
1 : √2 : √3 : 2 : √5 : √6 : √8 : 3
BCC
1 : √2 : √3 : 2 : √5 : √6 : √7 : √8 : 3
FCC
√3 : 2 : √8 : √11 : √12 : 4 : √19
HCPS
√32 : 6 : √41 : √68 : √96 : √113
DD
√2 : √3 : 2 : √6 : √8 : 3 : √10 : √11
Ia3̄d
√3 : 2 : √7 : √8 : √10 : √11 : √12
Pm3̄n
√2 : 2 : √5 : √6 : √8 : √10 : √12

Figure 1-1-3

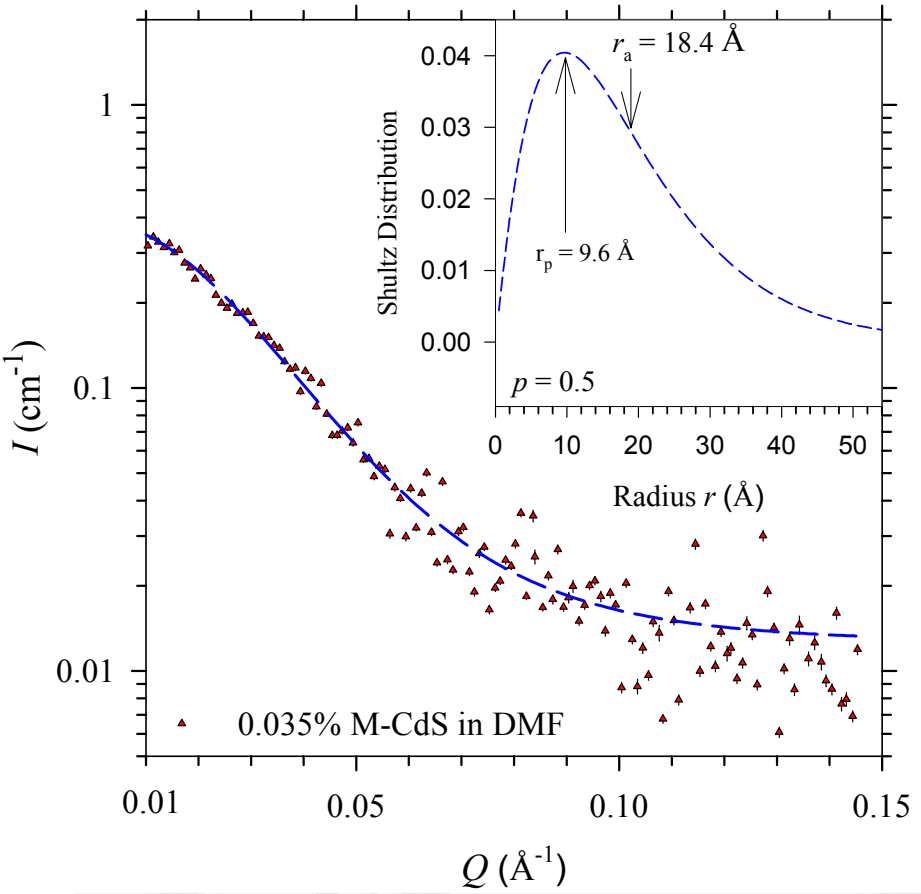
1
0.1
0.01
I (cm-1)
0.01
0.05
0.10
0.15
Q (Å-1)
0.035% M-CdS in DMF
Shultz Distribution
0.04
0.03
0.02
0.01
0.00
ra = 18.4 Å
rp = 9.6 Å
p = 0.5
0
10
20
30
40
50
Radius r (Å)

Figure 1-4-1

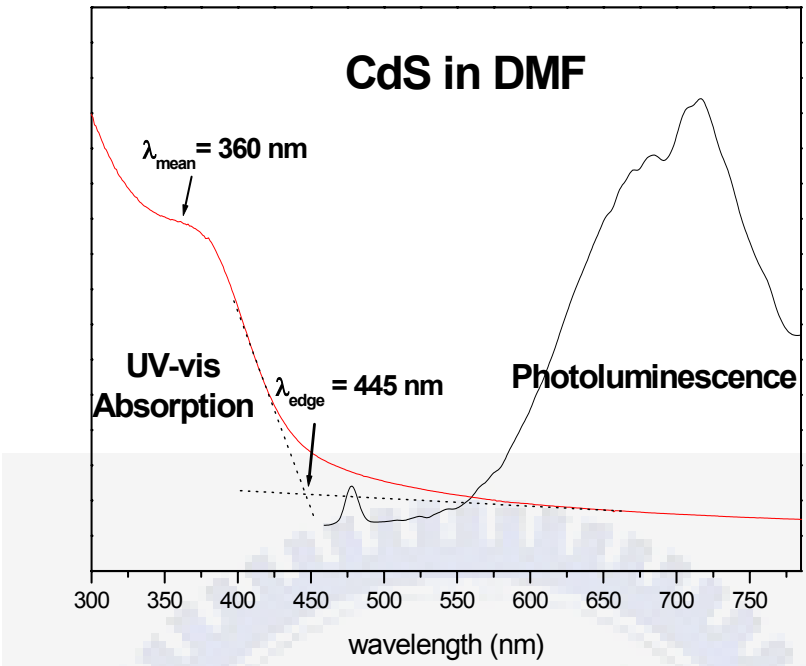

(a)

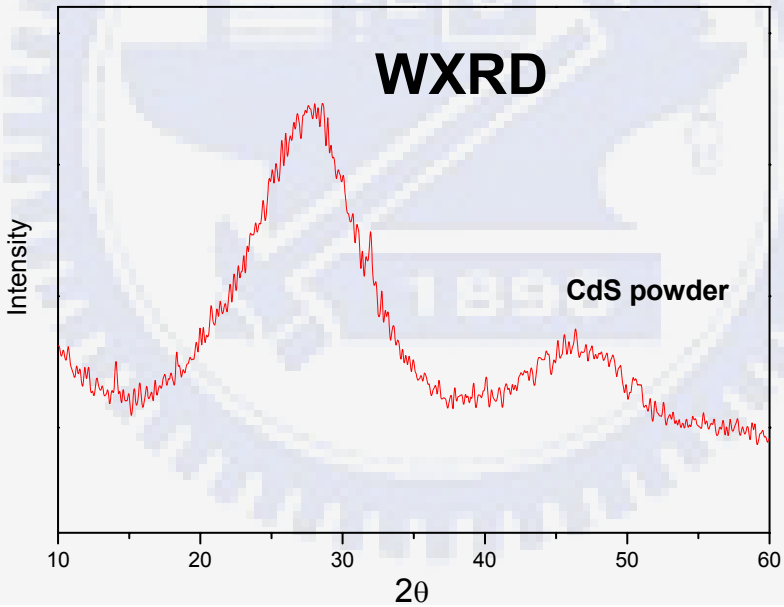

(b)

Figure 1-4-2

Chapter 2: Effects of CdS in SEO in Bulk Samples

2-1 Introduction

Block copolymers are versatile platform materials because they can self-assemble into various nanostructures with periodic thicknesses on the scale of tens to hundreds of nanometers under the appropriate compositions and conditions, owing to microphase separation between incompatible blocks.[1-4] The crystallization and morphology of one particular type of block copolymer, crystalline-amorphous diblock copolymers, have been studied extensively. For example, morphology and crystallization of asymmetric poly(styrene-b-ethylene oxide) (SEO),[5-6] poly(1,4-butadiene)-b-poly(styrene-r-butadiene), polyethylene-b-poly(vinylcyclohexane),[7] and poly(butadiene-b-ethylene oxide)[8,9] have been reported.

For semiconductor nanoparticles with sizes close to their Bohr exciton radius (typically between 1-10 nm), the size-dependent band gap results in tunable optical properties.[10-11] These semiconductor nanoparticles are termed as quantum dots because their tunable optical properties can be predicted by quantum mechanics. Nanoparticles that are not treated with a surfactant or bonded to polymer chains will, however, from large aggregates.

Recently, the use of nanostructured block copolymers as templates to selectively control the spatial location of semiconductor nanoparticles in one of the blocks may lead to several potential applications. For instance, periodic high refractive index contrast domains in phase-separated block copolymers can be used in photonic crystal applications.[12] Moreover, several groups have also reported the in-situ synthesis of Co, Ag, Pb,[13] $CoFe_2O_4$,[14] and CdS[15] nanoparticles or the ability to

control the spatial location of nanoparticles such as Au and SiO_2,[16] Pd,[17] , TiO_2, and CdS[18] by polystyrene-b-poly(ethylene propylene), polystyrene-b-poly(acrylic acid), polystyrene-b-poly(methylmethacrylate), polystyrene-b-poly(vinylpyridine) and SEO. The incorporation of nanoparticles into block copolymers, however, would lead to more complicated block copolymer morphologies than their pristine state as predicted by Balazs'group,[19] which used a self-consistent field theory and a density functional theory for describing the polymer and the nanoparticles, respectively, to predict the morphology and phase diagram. These studies motivated us to investigate the interaction between the block copolymer and nanoparticles, particularly on the effect of nanoparticles in the morphology of block copolymers.

In this part, we prepare self-assembled CdS/HSEO and CdS/LSEO nanocomposites in the bulk form and report the selective distribution of CdS nanoparticles in the PEO block of diblock copolymers, HSEO and LSEO, and the resultant morphological changes. Specifically, in the case of HSEO bulk samples, CdS nanoparticles induce the PEO domains to change from hexagonally-packed PEO cylinders to body-centered cubic or simple cubic CdS/PEO spheres, as shown in Scheme 2A-1. To our knowledge, this is the first study concerning the morphological transformation of block copolymer by nanoparticles. The binding of the nanoparticles leads to spherical PEO/CdS microdomains in the composites with a greatly enhanced thermal stability. In another case of CdS/LSEO, the effect of CdS nanoparticle concentration on the crystallization and morphology of hexagonally-packed cylindrical LSEO diblock copolymer is shown in Scheme 2B-1 and reported in detail.

2-2 Methods and Analysis

Two kinds of block copolymers, HSEO and LSEO, are involved in the

incorporation of CdS nanoparticles. Synthesis of CdS nanoparticles has been reported previously in the section 1-4. Proper ratios of CdS and SEO (HSEO or LSEO) were mixed in DMF. These mixtures were dried slowly under vacuum at 323 K and then maintained at 383 K for 24 h to obtain the CdS/HSEO and CdS/LSEO nanocomposites. Preparation of pure HSEO and LSEO bulks is similar to that of CdS/SEO except the lack of CdS. Thermal Gravity Analysis had been used to check the presence of the residual DMF solvent, and there was no residual DMF present in these block copolymer nanocomposites.

For morphological studies, small-angle X-ray scattering (SAXS), transmission electron microscopy (TEM) and atomic force microscopy (AFM) were used to determine the morphology of CdS/HSEO and CdS/LSEO bulk samples. SAXS experiments were performed on wiggler beamline BL-17B1 at the National Synchrotron Radiation Research Center, Taiwan. For TEM and AFM studies, the thin specimens were microtomed with Leica Ultracut Uct equipped with a diamond knife and subsequently deposited on copper grids and silicon wafers. TEM images were obtained with Hitachi H-600 transmission electron microscope operating at 100kV. AFM measurements were performed in taping-mode with a Digital Nanoscope IIIa under ambient conditions. In addition, the crystallization and thermal properties of the nanocomposites were measured by wide-angle X-ray diffraction (WXRD) and differential scanning calorimetry (DSC). WXRD on samples was collected by using a conventional rotating anode source. The glass transition temperatures (Tg) and melting point (Tm) were obtained from a Dupont DSC 2910 at a heating rate of 20℃/min. Fourier transformed Infrared spectroscopy (FTIR) spectra of the samples were obtained from a spectrometer of model Nicolet PROTÉGÉ-460. Photoluminescence spectra (PL) were obtained with a Hitachi F4500 fluorescence spectrophotometer at room temperature.

2-3 Results and Discussions

The effects of CdS nanoparticles on crystallization and morphological changes of HSEO and LSEO bulk samples are shown and discussed individually in the section 2-3-A for bulk CdS/HSEO and 2-3-B for CdS/LSEO.

2-3-A. CdS-induced morphological transformation of bulk HSEO

Figure 2A-1 shows one-dimension small-angle X-ray scattering patterns (SAXS) of HSEO and CdS/HSEO nanocomposites by synchrotron radiation. For pure HSEO, four peaks appear at Q = 0.016, 0.027, 0.032 and 0.042 Å $^{-1}$, corresponding to a ratio of 1:$3^{1/2}$:$4^{1/2}$:$7^{1/2}$. This ratio indicates typical scattering by hexagonally-packed cylinders (HEX). The inter-cylinder distance (*D*) was determined to be 45.3 nm by equation (1).

$$D = \left(4/3\right)^{1/2} * d_{100} \quad (1)$$

where $d_{100}=2\pi/Q_{100}$ and Q_{100}= 0.16 nm^{-1}. In the case of HSEO containing 3.5% CdS, the scattering peaks are located at Q = 0.0114, 0.0158, 0.0203, 0.0228, 0.0281 and 0.0399 Å $^{-1}$, which gives a ratio of 1: $2^{1/2}$:$3^{1/2}$:$4^{1/2}$:$6^{1/2}$:$12^{1/2}$. This ratio implies that the scattering is caused by either body-centered cubic packed spheres (BCC) or simple cubic spheres (SC). The inter-sphere distance is 67.5 nm, as determined from equation (2).

$$D = \left(3/2\right)^{1/2} * d_{110} \quad (2)$$

where $d_{110}=2\pi/Q_{110}$ and Q_{110}= 0.114 nm^{-1}. SAXS results confirm that the nanostructured HEX structure of pure HSEO has been transformed to a BCC or SC morphology, due to the presence of CdS Nanoparticles. The size of CdS Nanoparticles in the block copolymer is about 2.5 nm, as derived from the structure

form of the SAXS curve.

Figure 2A-2(a) and 2A-2(b) show the transmission electron microscopy (TEM) images of HSEO stained with OsO_4 and CdS/HSEO without staining, respectively. PEO domains appear in dark phase in Figure 2A-2(a), owing to selective staining, and display as short cylinders. In the case of CdS/HSEO, however, periodic dark spherical phases of CdS-included PEO appear, and no pure PEO domains without CdS Nanoparticles could be observed. The location of CdS in the PEO domain is revealed by energy dispersive spectrometry. Dark phases are caused by the higher electron density of cadmium relative to that of HSEO. The selective distribution of mercaptoethanol-modified CdS in the PEO domain is quite possibly due to dipole-dipole interactions between the hydroxyl groups of mercaptoethanol and the PEO block. The diameter of CdS-included PEO spheres is approximately 23 nm and the inter-sphere distance is about 60 nm, as estimated from their TEM images. In order to cover all PEO domains, there must be some distributions of CdS Nanoparticles in each PEO domain because the volume fraction of added CdS with respect to the PEO block is about 2.7%, which is not enough to cover each PEO domain fully. It is, however, not possible to detect them with the current techniques.

The results from TEM analysis are consistent with those by SAXS. Further evidence of the two different morphologies can be found in phase-contrast atomic force microscopy images (AFM) of HSEO and CdS/HSEO samples, as shown in Figure 2A-2(c) and 2A-2(d), respectively. A diamond knife used during the microtoming process causes the oblique lines in these figures. The difference in the images of pure HSEO by TEM and AFM (Fig. 2A-2(a) and 2A-2(c)) could be explained by the fact that the dark PEO domains which appear as inclined short cylinders in bulk can be projected into cylindrical shapes in the transmission electron microscopy study, whereas the topology of the same microtomed slice would shows

hairy spherical images by the tapping mode of AFM.

Figure 2A-3(a) shows the thermal analysis results of HSEO and CdS/HSEO by differential scanning calorimetry. A crystal melting peak at 42.9^{o}C associated with the PEO domain and a glass transition temperature (Tg) at 99 ^{o}C attributed to the PS domain appear in the pure HSEO case (the amorphous phase of PEO is rather small and undetectable). In the presence of CdS, the crystal melting peak of PEO depressed and diminished to a small kink, with an apparent Tg of -56.6 ^{o}C; The PS domain, however, maintains a Tg of about 99 ^{o}C. The difference between the two cases can be explained by a loss of crystallinity in the PEO domain by the infiltration of CdS nanoparticles into the PEO domain. Moreover, the WXRD results shown in Figure 2A-3(b) and 2A-3(c) also support the corresponding crystal-to-amorphous change of the PEO domain. In the case of pure HSEO, two sharp peaks at 2θ =19.0^{o} and 23.21 ^{o} represent the crystallinity peaks of the PEO domain after deconvolution, as shown in Figure 2A-3(b). Figure 2A-3(c) shows the decrease of crystallinity of PEO domain when CdS is incorporated into the PEO domain, indicating the change from crystalline to amorphous PEO. This result is also consistent with those obtained by DSC. The possible scenario for this phenomenon is due to the relatively small size of CdS to the contour length of PEO block (2.5nm vs. 130nm) and the dipole-dipole interaction between the angling hydroxy group of surface-attached mercaptoethanol on CdS and ethylene oxide in PEO domain, CdS are tethering to PEO chain and appears to destroy the crystallinity of PEO domain, as shown in Scheme 1. This enables CdS-infiltrated PEO domains to be amorphous and to minimize their surface energy by forming either BCC or SC structures.

When only the volume fraction of the block copolymer HSEO is considered, it is true that in the equilibrium state the pure HSEO should be in the spherical region with

body-center cubic packing due to strong segregation.[20] The morphology of asymmetric amorphous-crystalline block copolymers, however, depends on both the microphase separation of the two blocks and the crystallization kinetics of the crystallizable block as demonstrated in the work by de Jeu et al.[21] In their study, lamellar or hexagonally perforated lamellar structures of HSEO were obtained even though the volume fraction of HSEO indicates that it is typically within the morphological range of sphere or cylinders. In our study, the hexagonally-packed cylindrical morphology of HSEO represents a compromise between the microphase separation involving PS and PEO blocks and the crystallization kinetics of the PEO block.[20-21] The cylindrical morphology of pure HSEO is in a meta-stable state due to the fast crystallization of the PEO block. The addition of CdS quantum dots into the diblock copolymer inhibits the crystallization of PEO block. The resultant morphology of CdS/HSEO sample, therefore, is determined largely by the microphase separation involving PS block and CdS/PEO block, (i.e. the crystallization effect is no longer existing). Theoretically, it is possible to observe the morphological transformation of pure HSEO, providing two requirements are satisfied-at high temperature (far above Tm of PEO and Tg of PS) and long time (diffusion rate of polymer melt is very small). In reality, this phenomenon may not happen for pure HSEO since block copolymer might start to degrade if it were maintained at high temperature for too long.

In Figure 2A-4, we show the SAXS result for the 14%CdS/HSEO composite, measured at 200°C – a temperature much higher than the melting and glass transition temperatures of the PEO (~40°C) and PS (100°C) blocks, respectively.[25] At 200°C, the scattering peaks in the lower-Q region diminish largely, indicating the disordering of the PEO/CdS domains in the copolymer matrix. Whereas in the higher-Q region (dominated by the nanoparticles), the SAXS profile persists surprisingly well, both in

shape and intensity, revealing that the PEO/CdS domains are stable during the large temperature transition. Overall, the integrated scattering intensity for the composite film, $Q_{inv} = \int_0^\infty I(Q)Q^2 dQ$, remains nearly the same as that at room temperature, strongly suggesting that the degree of phase separation, $Q_{inv}/Q_{inv\text{-}ideal}$, between the PEO/CdS domains and the PS matrix, is inert to the temperature change. Here $Q_{inv\text{-}ideal} = 2\pi^2\eta(1-\eta)(\Delta\rho)^2$ is the integrated scattering intensity for an ideal two-phase system of sharp boundary, in our case, PEO/CdS domains in PS matrix. Despite the loss of the mesomorphic order at 200°C, the SAXS result shows that PEO/CdS domains persist, maintaining their individual integrity without disassociating into the PS matrix. This picture is indeed visualized in the corresponding TEM image (Figure 2A-6) taken for the structure frozen at 200°C.

In contrast, the scattering invariant, Q_{inv}, for the pure copolymer, of a PEO crystal melting temperature ~ 40°C, is very sensitive to temperature changes, and decreases quickly to only 18 % of that at room temperature (inset in Figure 2A-4), even upon a moderate temperature increase to 100°C (~ T_g of the PS block). Using the molecular weight and the volume fraction of the PS-b-PEO copolymer, we can also calculate a consistent order-disorder transition temperature T_{ODT} = 94 °C for the pure copolymer, basing on the temperature-dependent interaction parameter proposed by Zhu et al.[5] and the universal phase diagram by Leibler.[23]

Photoluminescence spectra of CdS nanoparticles in DMF and the CdS/HSEO nanocomposite film are shown in Figure 2A-5. CdS nanoparticles in DMF emit red light with a maximum intensity located at 650 nm. The peak maximum of CdS in the PEO block of HSEO is red-shifted by 30 nm compared to CdS in DMF. The red-shift in the luminescence of CdS nanoparticles might be caused by aggregation or the different chemical environment.[11]

In conclusion, semiconductor CdS nanoparticles can be selectively dispersed in the PEO domain of HSEO block copolymer by using a surfactant. The CdS-infiltrated PEO domains are transformed from originally hexagonally-packed cylindrical structures to BCC or SC structures because CdS inhibits the crystallization and minimizes the surface energy of CdS-infiltrated PEO phase. The photoluminescence of CdS is slightly affected by their incorporation in HSEO.

2-3-B. CdS-induced structural change of bulk LSEO

Figure 2B-1(a) shows differential scanning calorimetry (DSC) analysis results of CdS/LSEO with various amounts of incorporated CdS nanoparticles. A crystal melting peak (Tm_{PEO}) at 58°C, associated with the PEO domain, appears in the pure LSEO case, while the glass transition temperature (Tg_{PEO}) of the amorphous phase of PEO is undetectable. In the presence of 43% CdS nanoparticles, the crystallinity of the PEO domain reduces to 5 J/g from 55 J/g for the pure PEO domain, and Tm_{PEO} decreases to 42°C from 58°C for pure PEO in LSEO. Tg_{PEO} is -40°C where CdS content increases. The crystallinity X_C^{DSC} can be calculated from DSC curves by equation (3).

$$X_C^{DSC} = \frac{1}{w_{EO}}\left(\frac{\Delta H}{\Delta H_0}\right) \qquad (3)$$

where ΔH_0 refers to the heat of fusion for completely crystallized PEO (ΔH_0 = 200 J/g)[22], as shown in Table 2B-1. It indicates that CdS dispersed in PEO domains in LSEO hinders the crystallization of PEO domains. Moreover, the wide-angle X-ray diffraction results also support the corresponding crystal-to-amorphous change of the PEO domain in LSEO. Figure 2B-1(b) shows the WXRD curves of pure LSEO after deconvolution; two sharp peaks at 2θ=19.0° and 23.21 ° represent the crystalline peaks of the PEO domain. The WXRD curves

in Figure 2B-1(c) can be deconvoluted to determine the crystallinity, X_C^{WAXS}, and results are given in Table 2B-1. X_C^{WAXS} can be obtained by equation (4).

$$X_C^{WAXS} = \frac{1}{w_{EO}}\left(\frac{A_c}{A_c + A_a}\right) \qquad (4)$$

where w_{EO} is the weight fraction of PEO and A_c and A_a are the areas under the crystalline and amorphous peaks. The CdS diffraction peak has been deconvoluted and taken out from the PEO crystalline curves. This analysis shows that the crystallinity of the PEO domain decreases with an increasing amount of CdS, indicating the retardation of PEO crystallization by the CdS nanoparticles. This result is also consistent with those obtained by DSC. The decrease in crystallinity of the PEO domain and the loading of CdS nanoparticles lead to the swelling of CdS/PEO composite cylinders and an increase in the volume fraction of the CdS/PEO domain in LSEO.

To verify the intermolecular interactions between CdS nanoparticles and PEO block, the vibration spectra of CdS/PSEO in a selected region: C-O-C symmetric and asymmetric stretching (1200-1000 cm^{-1}) were obtained, as shown in Figure 2B-2, and the results were discussed in the following. In the presence of 7% to 43% CdS in PEO domains, the C-O-C stretch vibrations of PEO chains display a shift toward lower wavenumbers, from 1100 cm^{-1} to 1085 cm^{-1}. The changes in the intensity, sharp, and position of C-O-C stretching mode are associated with the interaction between PEO and surface-hydroxylated CdS nanoparticles, revealing the formation of dipole-dipole interactions between the oxygen atoms of PEO chains and hydroxyl groups on CdS nanoparticles.[23]

Figure 2B-3 shows one-dimension small-angle X-ray scattering (SAXS) patterns of CdS/LSEO nanocomposites with various CdS content by synchrotron radiation. For pure LSEO, four peaks appear at Q = 0.021, 0.041, 0.053 and 0.078 $Å^{-1}$,

corresponding to a ratio of $1:4^{1/2}:7^{1/2}:12^{1/2}$. This ratio indicates scattering by hexagonally-packed cylindrical (HEX) nanostructures. The inter-cylinder distance (D) was determined to be 35.07 nm using equation (5).

$$D = \left(4/3\right)^{1/2} * d_{100} \qquad (5)$$

where $d_{100}=2\pi/Q_{100}$ and $Q_{100}= 0.21\ nm^{-1}$. After incorporating CdS nanoparticles into the LSEO diblock copolymer, HEX nanostructures in CdS/LSEO still remain, but the ordering peaks of SAXS curves shift to a lower Q region, indicating an enlargement of the center-to-center distance between the PEO composite cylinders. The distance is measured from the center of a cylinder to that of a neighboring cylinder. The enlarged distance is a result of the reduced crystallinity and swollen CdS/PEO composite cylinders. A complete listing of inter-cylinder distances for various CdS/LSEO nanocomposites is given in Table 2B-2. From the SAXS curves, the increasing CdS content in LSEO leads to a reduction in the ordering peaks due to the convolution with CdS nanoparticle scattering contributions. In the case of CdS/LSEO with 43% CdS in the PEO block, the HEX PEO nanostructure is destroyed, which may be explained by the fact that CdS nanoparticles fill up a large fraction of free spacing in the PEO domains and alter the surface energy of the PEO composite domains in LSEO.

Figure 2B-4 shows TEM images of LSEO containing various amounts of CdS nanoparticles. In Figure 2B-4(a), the dark region is the PEO domain, due to staining by OsO_4, and the lighter region is the PS domain. The cylindrical nanostructure of pure LSEO is easily revealed. The diameter of the PEO cylinder is about 14 nm. There is no staining in Figures 2B-4(b)-(f); the darker color represents the PEO/CdS composite phase, because of the higher electron density of cadmium. The location of CdS in the PEO domain was probed by energy

dispersive spectrometry, and no PEO domains without CdS nanoparticles could be observed in LSEO. The selective distribution of mercaptoethanol-modified CdS in the PEO domain is likely due to dipole-dipole interactions between the hydroxyl groups of mercaptoethanol and the PEO block. In Figures 2B-4(b)-(e), the cylindrical morphology of CdS/LSEO nanocomposites is distorted when the amount of CdS nanoparticles in PEO phase is increased. The cylindrical nanostructure, however, was destroyed in high CdS content CdS/LSEO (43% CdS in PEO) as seen in Figure 2B-4(f), which is consisted with SAXS results.

Figure 2B-5 shows the comparison of photoluminescent properties of CdS in DMF and in PEO domains. After dispersing CdS selectively in the PEO domains of the PSEO block copolymer, the excitonic fluorescence diminishes, and apparent red broad surface-trapped luminescent characteristics largely remain unchanged. Moreover, the main broad surface-trapped fluorescence of CdS nanoparticles in PEO domains displays a slight blue shift to 711 nm from 717 nm when CdS content is low (7-28%), but displays a red shift to 715 nm at 43 % CdS content in PEO. The disappearance of the excitonic fluorescence and the blue shift of the broad surface-trapped fluorescence can be explained by the fact that the chemical environment of CdS nanoparticles has changed from amide groups (in DMF) to ethylene oxide groups (in PEO blocks). In the case of high CdS concentration (43%) in PEO domains, however, the CdS nanoparticles become agglomerated in the PEO domains and cause the red shift of the surface-trapped fluorescence.

To clarify the agglomeration of CdS nanoparticles in DMF and in the composites, the surfactant removal and its sequence in the process were given more detailed discussions. The surface-hydroxylated CdS nanoparticles were synthesized by bonding the surfactant, mercaptoethanol, to CdS nanoparticles with the thiol group, and then were dispersed and mixed with PSEO in DMF. The CdS/SEO

nanocomposite films were formed after drying under vacuum at 323 K and being maintained at 383 K for 24 h. During drying processes, the solvent, DMF, is removed and, in our opinion, a small ratio of mercaptoethanol may be also carried away from the CdS surface because the strong hydrogen bonding, between DMF and mercaptoethanol, and the lower boiling point of mercaptoethanol than that of DMF (157^{o}C vs. 165^{o}C). The removal of the surfactant from the surface of CdS nanoparticles causes their agglomeration and the broadening and red shift of their photoluminescent peaks. By comparing the photoluminescence of CdS/PSEO composites to that of CdS in DMF, the amount of surfactants that was removed seems to be small during drying processes because no red shift, only a little broadening, is shown in the photoluminescent peaks in Figure 2B-5.

In conclusion, CdS nanoparticles selectively dispersed in a PEO block hinder crystallization of PEO, resulting in an increase in the inter-cylinder distance of the HEX CdS/LSEO, as shown in Scheme 2B-1. High CdS nanoparticle concentration, however, destroys the ordered HEX nanostructure of LSEO. Furthermore, the comparison of photoluminescence of CdS in DMF and in PEO domains of PSEO block copolymers has been discussed in detail.

2-4 Conclusions

Surface-modified CdS nanoparticles selectively dispersed in a PEO block hinder crystallization of PEO and maintain their original optical properties in both cases of CdS/HSEO and LSEO bulk samples. Moreover, the CdS-infiltrated PEO domains, in the case of CdS/HSEO, are transformed from originally hexagonally-packed cylindrical structures to BCC or SC structures because of the inhibition of the crystallization in PEO and minimization of the surface energy of CdS/PEO domains. In the case of CdS/LSEO, however, segregation of CdS nanoparticles results in an

increase in the inter-cylinder distance of the HEX CdS/LSEO, but the ordered nanostructure of LSEO is destroyed by high CdS content.

Acknowledgment

We appreciate Drs Sun, Y. S.; Jeng, U. S.; Liang, K. S. in National Synchrotron Radiation Research Center discussions and experimental support, and the financial support of the National Science Council through project NSC 92-2120-M-009-009.

References

1. (a) Bates, F. S.; Fredrickson, G. H. Annu. Rev. Phys. Chem. 1990, 41, 525. (b) Bates, F. S. Science 1991, 251, 898.
2. Hamley, I. W. The Physics of the Block Copolymers, Oxford University Press: New York, 1998.
3. Lazzari, M.; Lopez-Quintela, M. A. Adv. Mater. 2003, 15, 1583.
4. Park, C.; Yoo, J.; Thomas E. L. Polymer 2003, 44, 6725.
5. (a) Zhu, L.; Huang, P.; Chen, W. Y.; Weng, X.; Cheng, S. Z. D.; Ge, Q.; Quirk, R. P.; Senador, T.; Shaw, M. T.; Thomas, E. L.; Lotz, B.; Hsiao, B. S.; Yeh, F; Liu, L. Macromolecules 2003, 36, 3180. (b) Zhu, L.; Cheng, S. Z. D.; Huang, P.; Ge, Q.; Quirk, R. P.; Thomas, E. L.; Lotz, B.; Hsiao, B. S.; Yeh, F; Liu, L. Polymer 2001, 42, 5829.
6. Li, L.; Serero,Y.; Koch, M. H. J.; de Jeu, W. H. Macromolecules 2003, 36, 529.
7. (a) Loo, Y. L.; Register, R. A.; Ryan A. J. Macromolecules 2002, 35, 2365. (b) Loo, Y. L.; Register, R. A.; Ryan A. J.; Dee, G. T. Macromolecules 2001, 34, 8968.
8. (a) Rottele, A.; Thurn-Albrecht, T.; Sommer, J. U.; Reiter, G. Macromolecules 2003, 36, 1257. (b) Reiter, G.; Castelein, G.; Sommer, J. U.; Rottele, A.;

Thurn-Albrecht, T. Phys. Rev. Lett. 2001, 87, 226101.

9. Chen, H. L.; Hsiao, S. C.; Lin, T. L.; Yamauchi, K.; Hasegawa, H.; Hashimoto, T. Macromolecules 2001, 34, 671.
10. (a) Veinot, J. G. C.; Ginzburg, M.; Pietro, W. J.; *Chem. Mater.* **1997**, *9*, 2117. (b) Herron, N.; Wang, Y.; Eckert, H.; *J. Am. Chem. Soc.* **1990**, *112*, 1322.
11. (a) Gao, M. Y.; Richter, B.; Kirstein, S.; *Adv. Mater.* **1997**, *9*, 802. (b) Gao, M. Y.; Richter, B.; Kirstein, S.; Mohwald, H.; *J. Phys. Chem. B* **1998**, *102*, 4096.
12. Urbas, A. M., Maldovan, M.; DeRege, P.; Thomas, E. L.; *Adv. Mater*. **2002**, *14*, 1850.
13. (a) Abes, J. J.; Cohen, R. E.; Ross, C. A. Chemistry of Materials 2003, 15, 1125. (b) Boontongkong, Y.; Cohen, R. E. Macromolecules 2002, 35, 3647.
14. (a) Ahmed, S. R.; Kofinas, P. Macromolecules 2002, 35, 3338. (b) Ahmed, S. R.; Ogale, S. B.; Papaefthymiou, G. C.; Ramesh, R.; Kofinas, P. Appl. Phys. Lett. 2002, 80, 1616.
15. (a) Moffitt, M.; Vali, H.; Eisenberg, A. Chemistry of Materials 1998, 10, 1021. (b) Moffitt, M.; McMahon, L.; Pessel, V.; Eisenberg, A. Chemistry of Materials 1995, 7, 1185.
16. Bockstaller, M. R.; Lapetnikov, Y.; Margel, S.; Thomas E. L. J. Am. Chem. Soc. 2003, 125, 5276.
17. (a) Ribbe, A. E.; Okumura, A.; Matsushige, K.; Hashimoto, T. Macromolecules 2001, 34, 8239. (b) Hashimoto, T.; Harada, M.; Sakamoto, N. Macromolecules 1999, 32, 6867.
18. (a) Weng, C. C.; Wei, K. H. Chemistry of Materials 2003, 15, 2936. (b) Yeh, S. W.; Wei, K. H.; Sun, Y. S.; Jeng, U. S.; Liang, K. S. Macromolecules 2003, 36, 7903.
19. (a) Thompson, R. B.; Ginzburg, V. V.; Matsen, M. W.; Balazs, A. C. Science

2001, 292, 2469. (b) Thompson, R. B.; Ginzburg, V. V.; Matsen, M. W.; Balazs, A. C. Macromolecules 2002, 35, 1060. (c) Lee, J. Y.; Shou, Z.; Balazs, A. C. Phys. Rev. Lett. 2003, 91, 136103.

20. Hamley, I. W. *The Physics of the Block Copolymers*, Oxford University Press: New York, 1998.
21. Li, L.; SereroY.; Koch, Michel H. J.; de Jeu, Wim H. *Macromolecules* **2003**, *36*, 529.
22. Floudas, G.; Tsitsilianis, C. Macromolecules 1997, 30, 4381.
23. Qiao, J.; Yoshimoto, N.; Ishikawa, M.; Morita, M. Chemistry of Materials 2003, 15, 2005.
24. Leiber, L. Macromolecules 1980, 13, 1602.
25. U. S. Jeng, Y. S. Sun, H. Y. Lee, C. H. Hsu, and K. S. Liang, S. W. Yeh, K. H. Wei, *Macromolecules* **2004**, *37*, 4617.

Scheme 2A-1 Morphological transformation of HSEO diblock copolymer by selectively dispersed colloidal CdS nanoparticles.

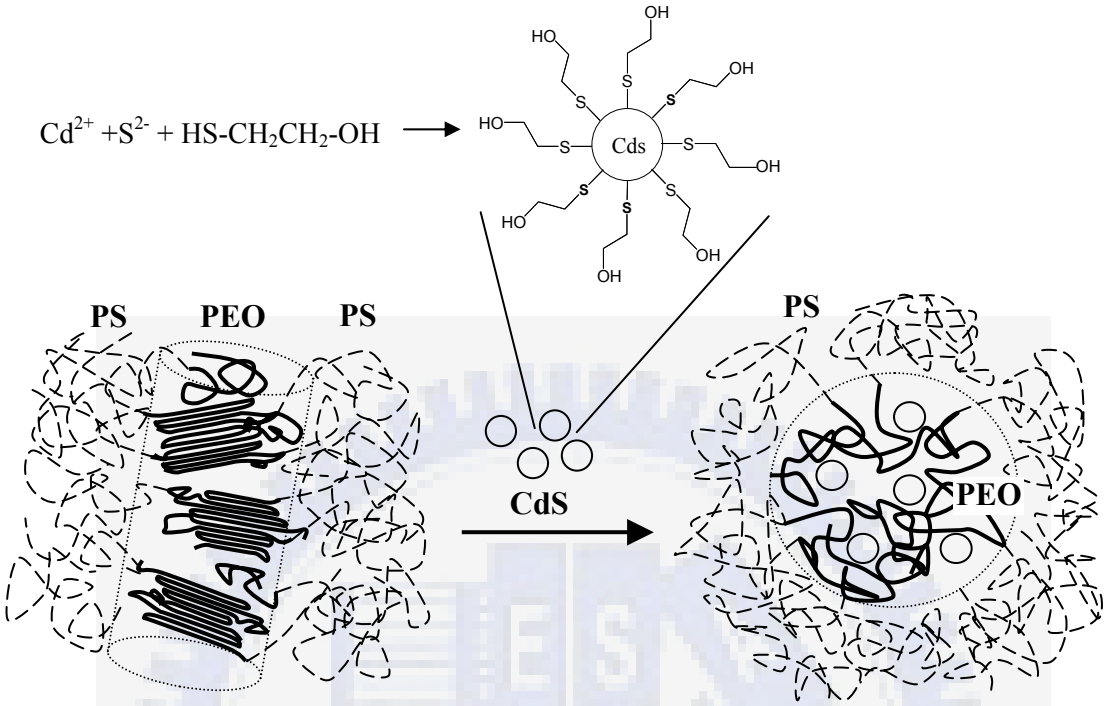

Figure Captions:

Figure 2A-1 Synchrotron SAXS curves of HSEO and CdS/HSEO.

Figure 2A-2 (a) TEM image of HSEO stained by OsO_4. The dark regions correspond to PEO phases stained with OsO_4. (b) TEM image of CdS/HSEO without staining. (c) AFM images of thin films microtomed from bulk HSEO and (d) AFM images of thin films microtomed from bulk CdS/HSEO.

Figure 2A-3 (a) DSC analysis of CdS/HSEO and HSEO. The samples were heated from -90^{o}C to 130^{o}C at 10^{o}C/min. (b) Deconvolution curves of the WXRD curve of crystallinity HSEO. (c) WXRD of HSEO and CdS/HSEO after crystallization at -20^{o}C for 18 hr.

Figure 2A-4 Comparison of SAXS profiles for the 14%CdS/HSEO composite measured at 30 °C and 200 °C, respectively. The inset shows SAXS data measured for the pure HSEO copolymer at 30 °C and 100 °C. Note that at 100°C, the profile of the pure copolymer is structureless after $Q \sim 0.06$ Å^{-1}.

Figure 2A-5 Photoluminescence of CdS and CdS/HSEO after excitation with 430-nm light.

Figure 2A-6 TEM images for the 14%CdS/HSEO composite at 200°C. The dark spherical regions are the PEO/ CdS domains. The bar represents a unit length of 100 nm for the image.

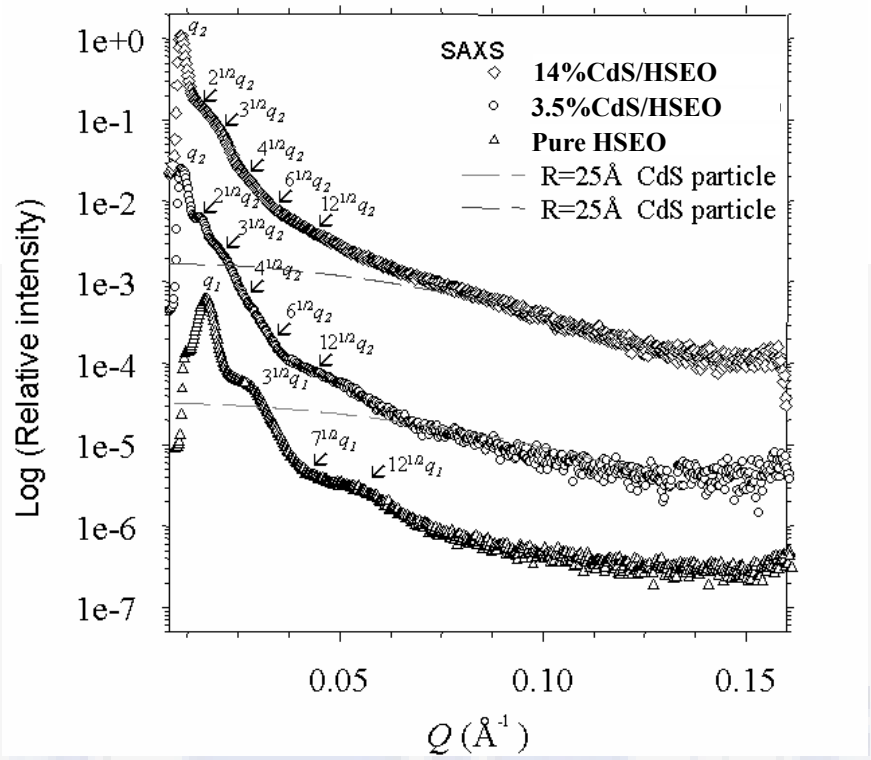
SAXS
14%CdS/HSEO
3.5%CdS/HSEO
Pure HSEO
R=25Å CdS particle
R=25Å CdS particle
Log (Relative intensity)
1e+0
1e-1
1e-2
1e-3
1e-4
1e-5
1e-6
1e-7
0.05
0.10
0.15
Q (Å-1)
q2
21/2q2
31/2q2
41/2q2
61/2q2
121/2q2
q1
31/2q1
71/2q1
121/2q1

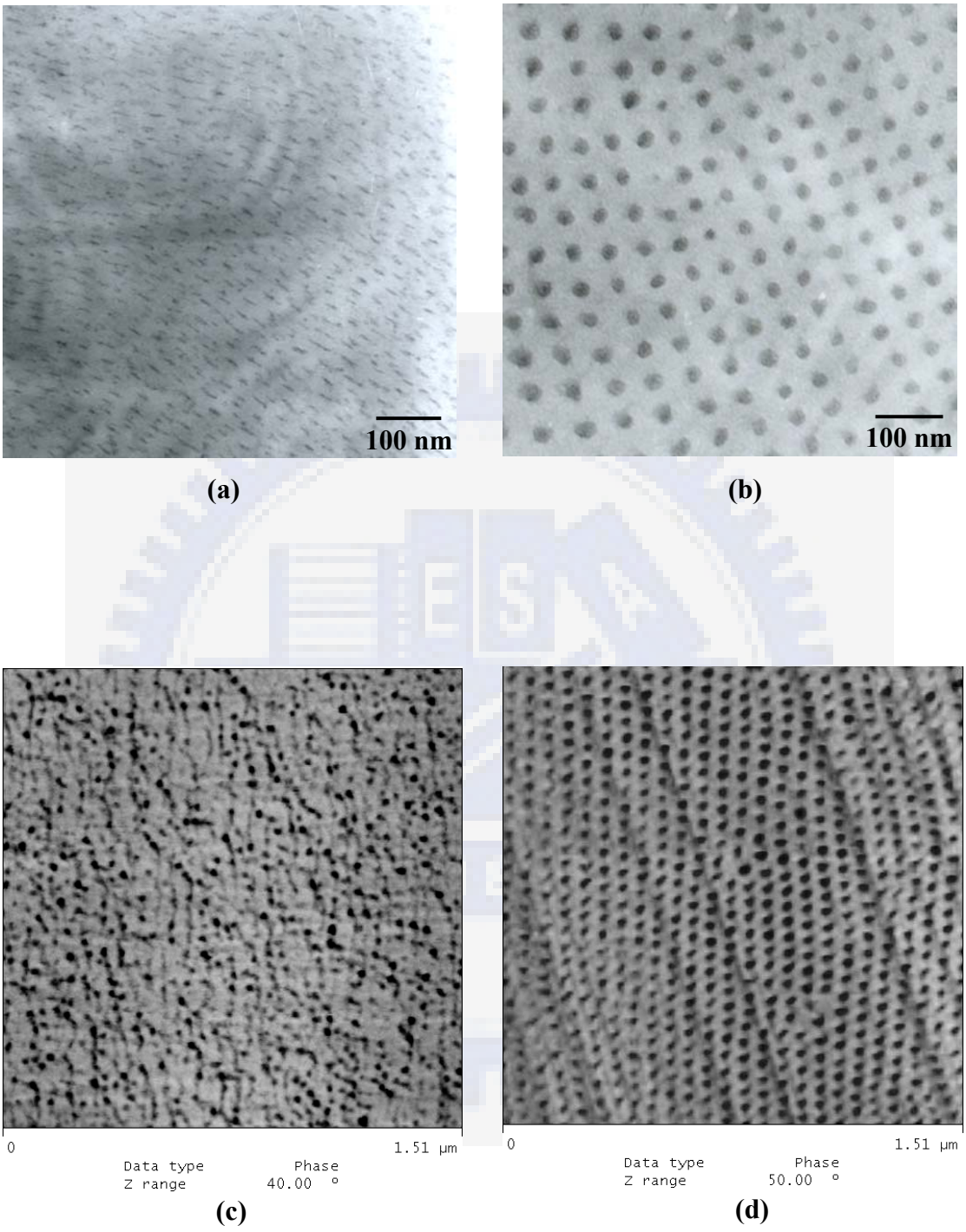
100 nm
100 nm
(a)
(b)
0
1.51 µm
Data type Phase
Z range 40.00 °
0
1.51 µm
Data type Phase
Z range 50.00 °
(c)
(d)

Figure 2A-2

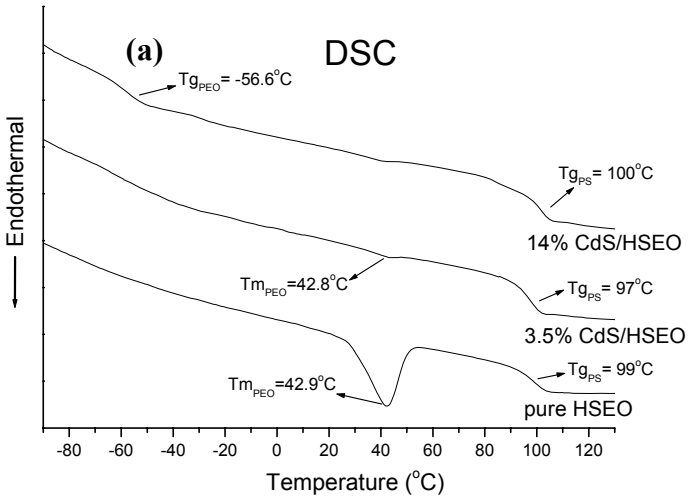
(a)
DSC
Tg$_{PEO}$= -56.6°C
Tg$_{PS}$= 100°C
14% CdS/HSEO
Tm$_{PEO}$=42.8°C
Tg$_{PS}$= 97°C
3.5% CdS/HSEO
Tm$_{PEO}$=42.9°C
Tg$_{PS}$= 99°C
pure HSEO
Endothermal
Temperature (°C)

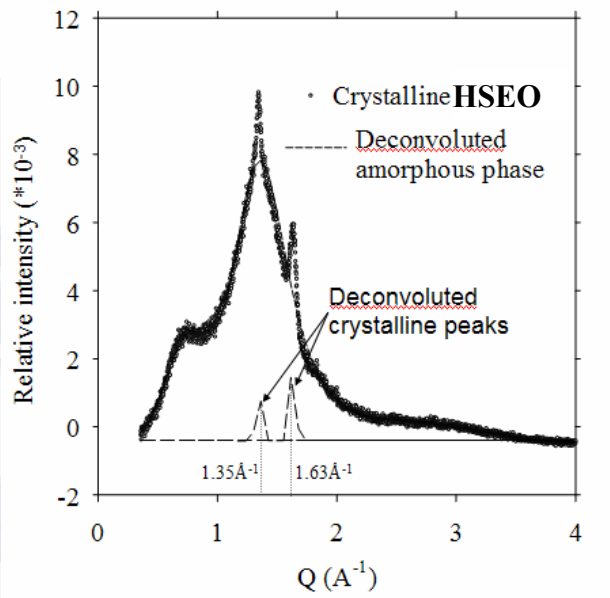
Crystalline HSEO
Deconvoluted amorphous phase
Deconvoluted crystalline peaks
1.35Å^{-1}
1.63Å^{-1}
Relative intensity (*10^{-3})
Q (A^{-1})

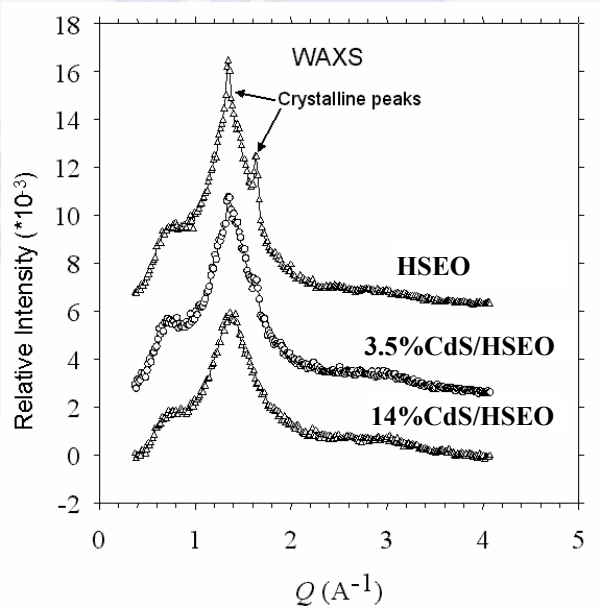
WAXS
Crystalline peaks
HSEO
3.5%CdS/HSEO
14%CdS/HSEO
Relative Intensity (*10^{-3})
Q (A^{-1})

Figure 2A-3

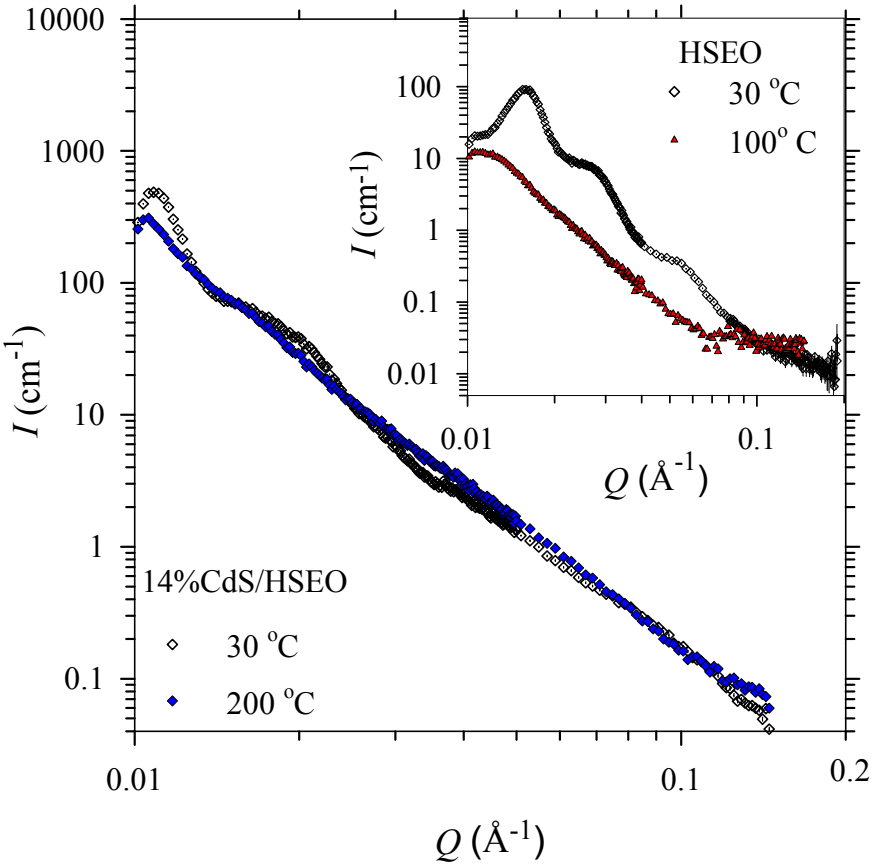
10000
1000
100
10
1
0.1
I (cm-1)
0.01
0.1
0.2
Q (Å-1)
14%CdS/HSEO
30 °C
200 °C
HSEO
30 °C
100° C
100
10
1
0.1
0.01
I (cm-1)
0.01
0.1
Q (Å-1)

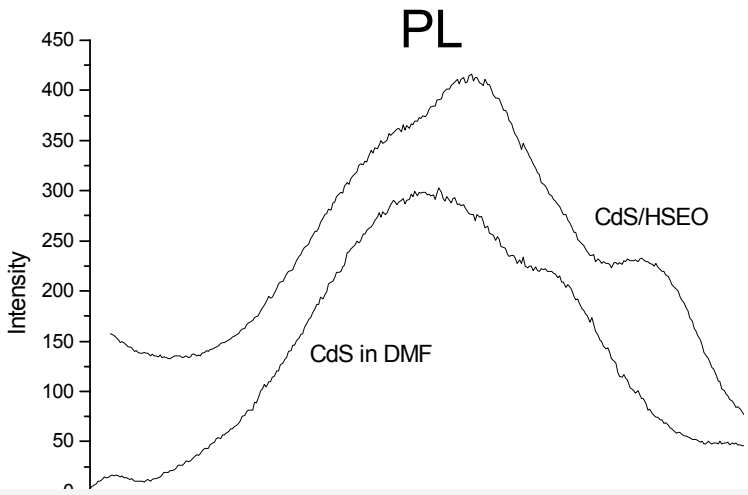
PL
Intensity
450
400
350
300
250
200
150
100
50
CdS/HSEO
CdS in DMF

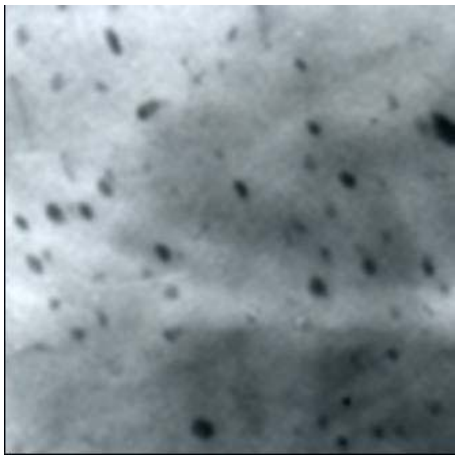
100nm

Scheme 2B-1 Crystalline and morphological properties of CdS/LSEO with various CdS content

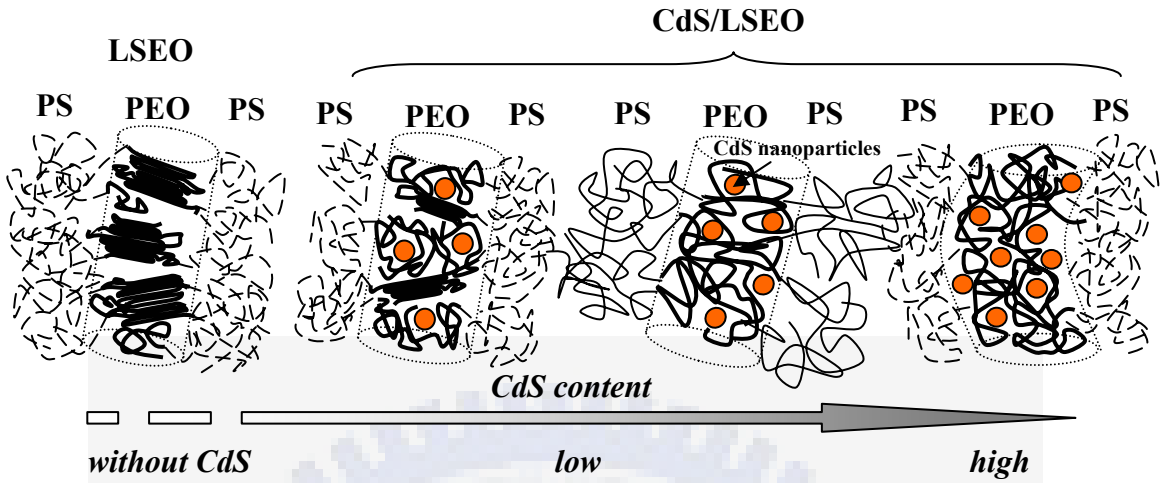

Table 2B-1 Crystallinity of CdS/PEO composites with various CdS content from DSC and WAXS results

CdS/PSEO	Crystallinity(X_C^{DSC}) of CdS/PEO composites [a]	Crystallinity(X_C^{WAXS}) of CdS/PEO composites [b]
0% CdS/LSEO	0.69	0.72
7% CdS/LSEO	0.48	0.53
14% CdS/LSEO	0.35	0.28
28% CdS/LSEO	0.07	0.13
43% CdS/LSEO	0.06	0.00

[a] X_C^{DSC} was calculated from DSC curves by equation (3).

[b] X_C^{WAXS} was calculated from WAXS curves after deconvolution by equation (4).

Figure Captions

Figure 2B-1: (a) DSC, (b) and (c) X-ray diffraction curves of CdS/LSEO with various CdS nanoparticle content.

Figure 2B-2: FTIR spectra of the CdS/PSEO in a selected region: C-O-C symmetric and asymmetric stretching (1200-1000 cm^{-1}).

Figure 2B-3: Small-angle X-ray scattering of CdS/LSEO nanocomposites with various CdS nanoparticle content.

Figure 2B-4: TEM images of (a) LSEO stained with OsO_4, (b) 7% CdS/LSEO, (c) 14% CdS/LSEO, (d) 28% CdS/LSEO, and (e) 43%/LSEO.

Figure 2B-5: Photoluminescence spectra of CdS nanoparticle in DMF and CdS/LSEO with various CdS nanoparticle content.

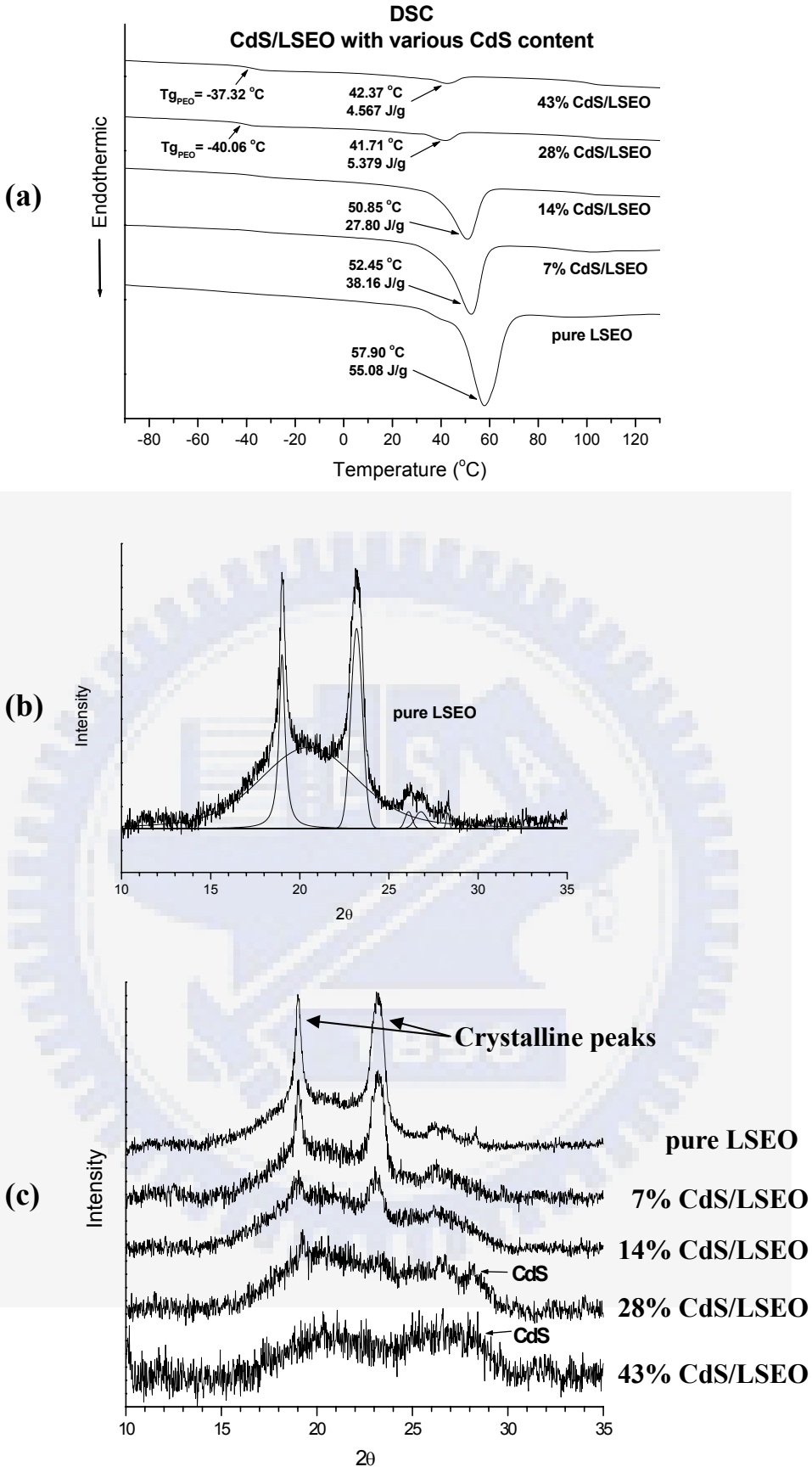
(a)
DSC
CdS/LSEO with various CdS content
Endothermic
Tg$_{PEO}$= -37.32 °C
42.37 °C
4.567 J/g
43% CdS/LSEO
Tg$_{PEO}$= -40.06 °C
41.71 °C
5.379 J/g
28% CdS/LSEO
50.85 °C
27.80 J/g
14% CdS/LSEO
52.45 °C
38.16 J/g
7% CdS/LSEO
pure LSEO
57.90 °C
55.08 J/g
-80 -60 -40 -20 0 20 40 60 80 100 120
Temperature (°C)
(b)
Intensity
pure LSEO
10 15 20 25 30 35
2θ
(c)
Intensity
Crystalline peaks
pure LSEO
7% CdS/LSEO
14% CdS/LSEO
CdS
28% CdS/LSEO
CdS
43% CdS/LSEO
10 15 20 25 30 35
2θ

Figure 2B-1

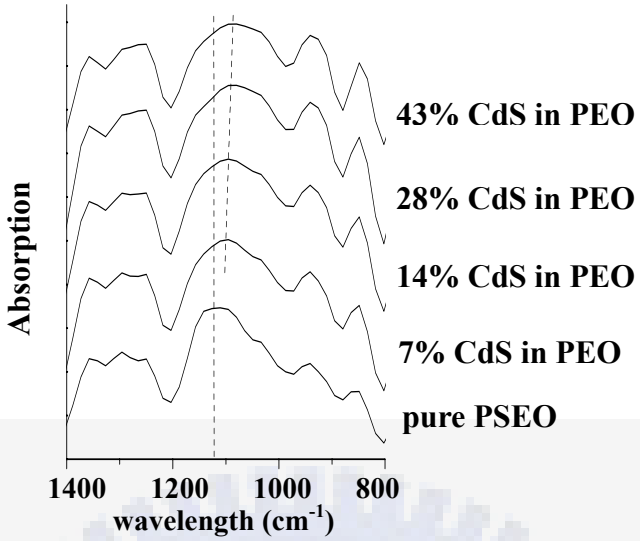
Absorption
43% CdS in PEO
28% CdS in PEO
14% CdS in PEO
7% CdS in PEO
pure PSEO
1400
1200
1000
800
wavelength (cm-1)

Figure 2B-2

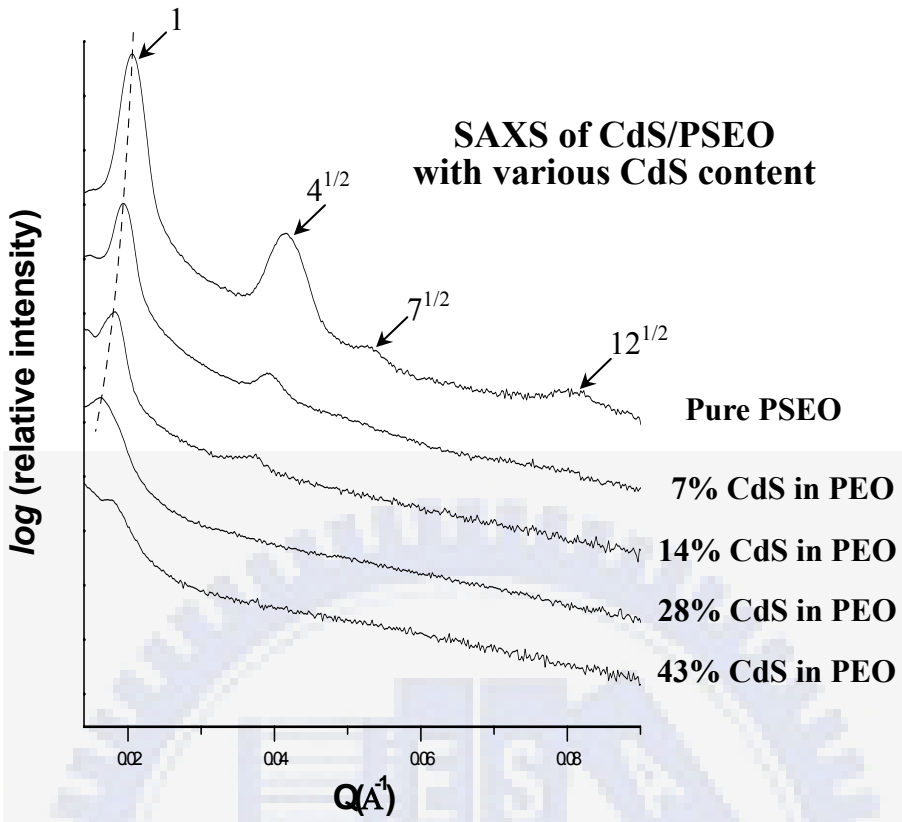
1
4^1/2
7^1/2
12^1/2
SAXS of CdS/PSEO
with various CdS content
log (relative intensity)
Pure PSEO
7% CdS in PEO
14% CdS in PEO
28% CdS in PEO
43% CdS in PEO
0.02
0.04
0.06
0.08
Q(A^-1)

Figure 2B-3

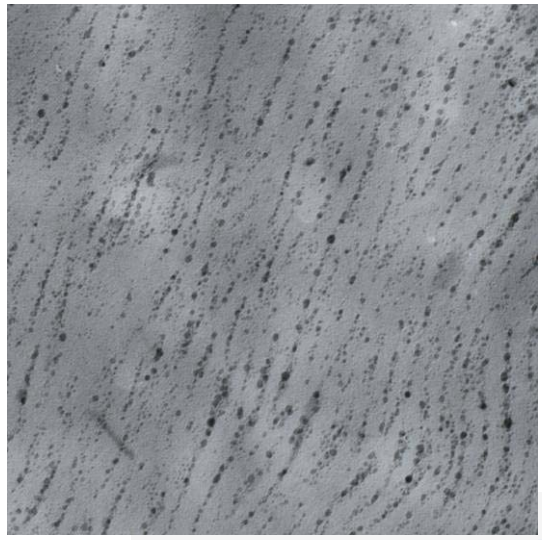

(a) 100 nm

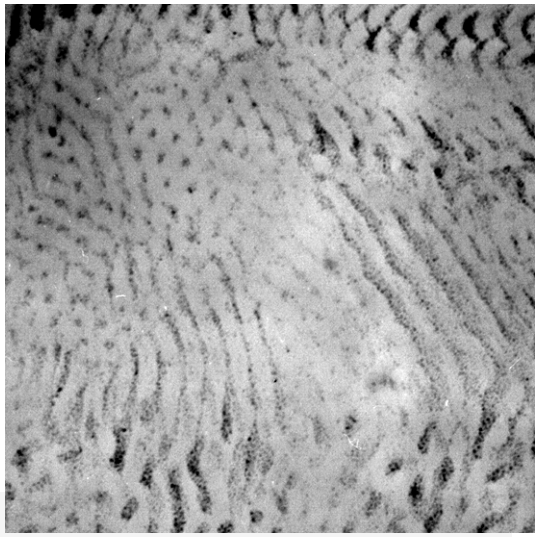

(b) 100 nm

(c) 100 nm

(d) 100 nm

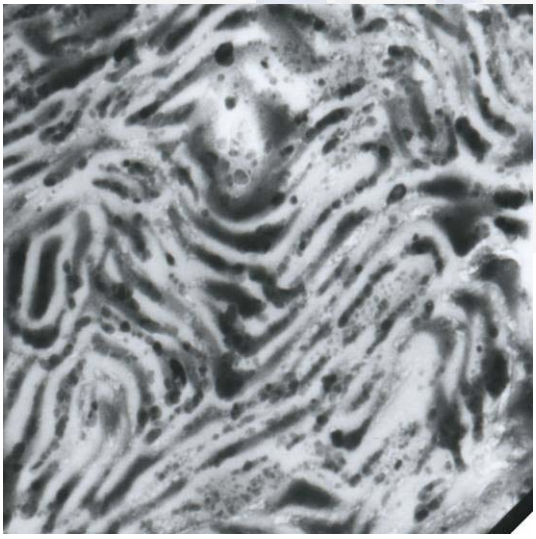

(e) 100 nm

Figure 2B-4

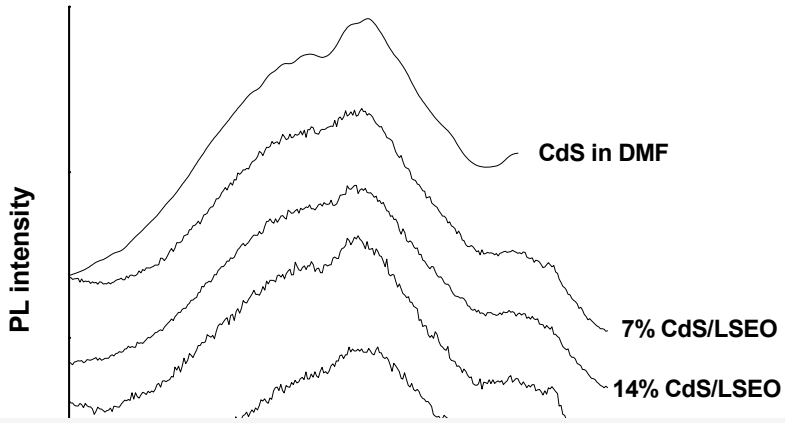

Figure 2B-5

Chapter 3: Effects of CdS in SEO Thin Films

3-1 Introduction

The fabrication of periodically ordered, two-dimensional nanostructures on the scale of ten to a hundred nanometers is critically important as electronic and magnetic devices are continually miniaturized. Block copolymers are versatile platform materials because they can self-assemble into various nanostructures with period thicknesses between 10 to 100 nm, under the appropriate compositions and conditions, owing to microphase separation between incompatible blocks.[1-10] Hence, self-assembled block copolymers in bulk form serve as good carriers for bringing nanoparticles into an ordered nanostructure.[11-15] A large morphological variety of block copolymers incorporated with nanoparticles has been observed, creating an interesting area of research. More complicated block copolymer morphologies, involving the incorporation of nanoparticles into block copolymers, have been predicted by Balazs'group,[16] which has used self-consistent field theory and density functional theory to describe the polymer and the nanoparticles, respectively; they have been able to predict the phase diagram and morphological structure of both systems. In our laboratory, the selective sequestration of pre-synthesized surface-modified CdS and TiO_2 nanoparticles into one block of polystyrene-b-poly(ethylene oxide) (SEO) and PS-b-PMMA block copolymers has been performed, respectively. The morphological transformation of bulk CdS/SEO with a higher molecular weight of SEO (PS/PEO = 125k/16.1k, volume fraction of PEO = 0.11) is also observed in Chapter 2.[17a, 17c] Moreover, CdS preferentially binds the poly(ethylene oxide) (PEO) block of the SEO block copolymer. The binding of nanoparticles promotes the segregation of the PEO/nanoparticles leading to spherical

CdS/PEO microdomains in the composite film with a greatly enhanced thermal stability.[17b]

On the other hand, diblock copolymer thin films (less than 100 nm) can be used to control the spatial position of nanoparticles via nanostructured block copolymers; a common approach has been to synthesize the nanocrystal clusters within micro-phase-separated diblock copolymer films. Using a polystyrene-b-polyvinylpyridine (PS-b-PVP) micellar solution, ordered Au clusters,[18] Co and Fe arrays,[19] and self-assembly of both Au and Fe_2O_3 nanoparticles[20] have all been synthesized. This approach is limited in its ability to control the optoelectronic or magnetic properties of the nanoparticle arrays due to constraints imposed by the polymer matrix. High density nanostructures of silicon nitride, GaAs[21], Au/Cr[22a] and magnetic cobalt dots[23] have been fabricated using polystyrene-b-polybutadiene, polystyrene-b-poly(methyl methacrylate) (PS-b-PMMA) and polystyrene-b-poly(ferrocenyldimethylsilane) block copolymers as lithographic templates. Au, Ag[24] and magnetic Co[22b] nanowires can also be produced using a PS-b-PMMA block copolymer template. Recently, another method using block copolymer thin films as templates to control the spatial arrangement of pre-synthesized nanoparticles has been reported. Russell et al. were able to screen different sizes of pre-synthesized CdSe nanoparticles with a nanoporous PS-b-PMMA template by capillary force.[25] Schrock et al. sequestered CdSe nanoclusters within phosphine-containing domains of a diblock copolymer.[26]

To our knowledge, the sequestration of pre-synthesized nanoparticles in thin block copolymer films through dipole-dipole interactions between the ligands on nanoparticles and a particular block have not yet been reported. In this chapter, we report a method to fabricate an ordered spatial arrangement of pre-synthesized nanoparticles in thin block copolymer templates by first selectively dispersing these

nanoparticles in one particular block of a diblock copolymer, in bulk, and then using solvent selectivity to sequester CdS nanoparticles in the block copolymer thin film, as shown in scheme 3A-1. This method can provide more flexibility in choosing a particular domain for nanoparticles containing matched surface ligands in a block copolymer thin film. The distance between nanoparticles is tuned by varying the molecular weight of the other block of the diblock copolymer. Moreover, substrates with shallow grooves are used to confine the nanocomposites for a long-range-order morphology study. On the other hand, we prepare CdS/SEO thin films, sequestered with CdS clusters in the PEO domains of the SEO block copolymer, and investigate the effects of hydrogen bonding between surface-hydroxylated CdS and ethylene oxide on the morphological transformation of CdS/SEO thin films from cylindrical PEO structures into spherical CdS/PEO domains, as shown in scheme 3B-1.

3-2 Methods and Analysis

The bulk CdS/HSEO and CdS/LSEO nanocomposites, as shown in chapter 2, were used for the thin film studies. 1 wt% micellar solutions of CdS/HSEO or CdS/LSEO were prepared by dissolving bulk CdS/HSEO or CdS/LSEO in dried toluene. Then, the micellar solutions were spin-coated at 5000 rpm for 60 sec on carbon-coated silicon wafers. After drying, the thin films were characterized by atomic force microscopy (AFM). During the initial stage to segregate CdS in the PEO domains of bulk CdS/SEO nanocomposites, both mercaptoethanol-modified CdS nanoparticles and the SEO block copolymer are dissolved in DMF, which is a good solvent for the PEO domain. CdS nanoparticles are therefore selectively dispersed into the PEO domains after evaporation of DMF. The CdS nanoparticles in each PEO domain are defined as a CdS cluster in this study. Subsequently, by using solvent selectivity, toluene, which is a good solvent for PS but a poor one for PEO, is

used to form micelles with CdS/PEO-core and PS-shell structures in the solution. This micellar solution is then spin-coated on a carbon-coated silicon wafer to form a thin film. The procedure to prepare ordered CdS nanoparticles in a thin block copolymer template is demonstrated in Scheme 1.

For morphological studies, AFM, TEM and SEM were used to characterize the thin film morphology. AFM measurements were performed in tapping-mode with a Digital Nanoscope IIIa under ambient conditions. TEM samples of monolayer-thin films on carbon-coated silicon wafers were prepared by removing the film from the wafer with 1% HF solution and depositing it on a copper net. TEM images were obtained with a Hitachi H-600 microscope. Scanning electron microscopy (SEM) images were obtained with a Thermal Field Emission Scanning Electron Microscope (JSM-6500F). In addition, the hydrogen bonding between CdS nanoparticles and ethylene oxide units were demonstrated by ^{1}H NMR and 2-D ^{1}H-^{13}C NMR spectra for hydrogen bonding studies were recorded on a Varian Unity-300 MHz NMR spectrometer by dissolving pure SEO and CdS/SEO samples in ^{8}d-toluene. Fourier-transformed infrared spectroscopy (FTIR) spectra of the thin films were obtained from a Perkin-Elmer Spectrum One FTIR spectrometer. Photoluminescence spectra (PL) were obtained with a Hitachi F4500 fluorescence spectrophotometer at room temperature.

3-3 Results and Discussions

The fabrication of pre-synthesized CdS cluster arrays in SEO thin films and the effects of CdS nanoparticles on morphological changes of CdS/LSEO thin films are shown and discussed individually in the section 3-3-A and 3-3-B.

3-3-A. Fabrications of ordered CdS clusters in CdS/SEO thin films

The procedure to prepare ordered CdS nanoparticles in a thin block copolymer template is demonstrated in Scheme 3A-1. During the initial stage, both mercaptoethanol-modified CdS nanoparticles and the SEO block copolymer are dissolved in DMF, which is a good solvent for the PEO domain. CdS nanoparticles are therefore selectively dispersed into the PEO domains after evaporation of DMF. Two cases of SEO are involved in the incorporation of CdS nanoparticles; they are CdS/HSEO and CdS/LSEO nanocomposites. The CdS nanoparticles in each PEO domain are defined as a CdS cluster in this study. Subsequently, by using solvent selectivity, toluene, which is a good solvent for PS but a poor one for PEO, is used to form micelles with CdS/PEO-core and PS-shell structures in the solution. This micellar solution is then spin-coated on a carbon-coated silicon wafer to form a thin film.

As shown in Figure 2A-2(b) and 2A-3(a), the TEM image and the DSC results indicate that CdS nanoparticles are selectively dispersed in the PEO phase due to dipole-dipole interactions between the hydroxyl groups of mercaptoethanol and ethylene oxide. The thin film fabrication is carried out by dissolving CdS/HSEO or CdS/LSEO in toluene to form a micellar solution, which is then dried in air. Figure 2 shows AFM and TEM images of a thin film of CdS/HSEO. In Figure 3A-1(a), 30 to 40 nm dark regions, representing ordered CdS-included PEO domains, appear in the height and phase contrast images. The inter-domain distance ranges from 120 to 140 nm. This also indicates that the microphase-separated CdS/HSEO thin film forms a monolayer thin film, since the thickness of the CdS/HSEO thin film is smaller than the size of the PEO domains (24.7 vs. 30 nm). Figure 3A-1(b) shows a TEM image of the CdS/HSEO thin film after it is removed from the carbon-coated silicon wafer with 1% HF solution. In Figure 3A-1(b), there are three distinct regions. The lightest regions, having circular shapes, are PEO domains, and the darkest regions

located within the PEO domains are CdS nanoclusters. The matrix, which appears as an intermediate gray, is the PS domain. The contrast in the three domains is caused by differences in the electron density of Cd, ethylene oxide, and styrene. The TEM image shows conclusively that CdS nanoparticles are located mostly within the PEO domain, but close to the interface between PEO and PS domains of the monolayer film, and that the distance between CdS clusters in the nanostructure is about 130 nm. The formation of the structure does not depend sensitively on the film thickness. Thin monolayer films are easier to characterize, and have greater potential for optical applications.

In the case of a lower molecular weight PS block in LSEO, similar patterns appear, but again with a difference. Figure 3A-2(a) shows the topology of the CdS/LSEO thin film in height and phase contrast images. Owing to the similar molecular weight of the PEO block in LSEO and HSEO, the size of the CdS-included PEO phase of the CdS/LSEO thin film is about 35 nm, which is close to that in the case of CdS/HSEO. The CdS/LSEO thin film is also a monolayer film because the thickness of the thin film of CdS/LSEO is about 30 nm. Figure 3A-2(b) shows a TEM image of the CdS/LSEO monolayer thin film after it is removed from the carbon-coated silicon wafer. The inter-domain distance between CdS-included PEO domains, however, is smaller than that in the CdS/HSEO thin film (70 vs. 130 nm), due to the smaller molecular weight of the PS block in LSEO.

Close examination of both Figure 3A-1(b) and 3A-2(b) reveals that some CdS nanoparticles are not located in the center of the PEO domains, but instead appear at the interface. Moreover, these CdS nanoparticles seem to clump together in the PEO domains. This can be explained by the fact that there are two types of dipole-dipole interaction forces involved in the nanocomposite system. The first type is due to mutual dipole-dipole attractions between the hydroxyl groups of mercaptoethanol on

CdS nanoparticles. The second type occurs between the free hydroxyl groups of mercaptoethanol on CdS and poly(ethylene oxide). CdS nanoparticles clump together by the first type of dipole-dipole interaction, but small CdS clusters disperse in the PEO domain by the second type of dipole-dipole interaction. A few portions of CdS nanoparticles are not fully within the PEO domain and a small fraction of CdS close to the interface may be due to a reduction in interfacial energy[15, 22(c)] and the excluding effect brought by some small crystallization in the PEO domain.

Long-range order in the block copolymer has been obtained by using substrate templating methods,[30, 31, 32] but no previous experimental study on nanoparticles/block copolymers has been carried out. We have used substrates consisting of thermally-oxidized silicon, patterned with square-wave profile grooves (400 nm in width and 40 nm in depth), produced using electron beam lithography and reactive ion etching. Figure 3A-3 shows phase contrast AFM images of an as-spun CdS/LSEO film on a patterned substrate containing these grooves. CdS/PEO domains within the 400-nm wide grooves orient parallel to the side of the groove, indicating a long-range order of the nanocomposite has been obtained. The size of the CdS/PEO domains is about 36 nm. The distance between confined CdS/PEO domains within the grooves is about 55 nm, which is slightly smaller than that of CdS/PEO on the smooth substrate.

Figure 3A-4 shows photoluminescence spectra of CdS in DMF and thin films of CdS/HSEO, CdS/LSEO, and pure LSEO. The photoluminescence of CdS nanoparticles has been reported previously in section 2-3-B. CdS clusters sequestered in PEO domains of CdS/HSEO and CdS/LSEO thin films appear to retain their luminescence characteristics, as compared to those in DMF. The main peak occurs at a wavelength of 715 nm, and it is caused by defects in CdS. The minor peak at 818 nm may be due to another defect in the CdS nanoparticles or pure SEO.

3-3-B. The effects of CdS nanoparticles on morphological changes of CdS/LSEO thin films

In this section, we prepare CdS/LSEO thin films, sequestered with CdS clusters in the PEO domains of the LSEO block copolymer, and investigate the effects of hydrogen bonding between surface-hydroxylated CdS and ethylene oxide on the morphological transformation of CdS/LSEO thin films from cylindrical PEO structures into spherical CdS/PEO domains, as shown in scheme 3B-1. Figure 3B-1(a), (b), (c), and (d) show phase contrast AFM images and TEM images of ca. 40-nm thick SEO thin films containing different amounts of CdS nanoparticles on carbon-coated silicon wafers. Figure 3B-1(e) shows an SEM cross-sectional image of 28 wt.-% CdS nanoparticles in SEO thin film on the silicon wafer after immersion in water. In the phase contrast AFM images, dark and light regions represent amorphous PEO and PS domains, respectively, due to the difference in the viscoelastic response of these materials. In TEM images of pure SEO without staining, however, PEO and PS domains are revealed as bright and dark regions, respectively, because of the greater electron density in styrene. In Figure 3B-1(a), the pure SEO thin film consists of PEO cylinders, 18 nm in diameter, dispersed in a PS matrix. This morphology is largely determined by the volume fraction of the PEO block. The average length of PEO cylinders is larger than 300 nm. In Figure 3B-1(b), the presence of 7 wt.-% CdS induces a small fraction of PEO domains to become spherical, as seen in the AFM image; the majority of PEO domains, however, remain cylindrical in shape, with lengths ranging from 200 to 300 nm. A close examination of the PEO domains shows that dark CdS clusters are selectively dispersed in the spherical PEO domains, with PEO cylinders remaining in a pure state. The average size of PEO cylinders and CdS/PEO spheres in CdS/SEO thin films with

various CdS contents are given in Table 3B-1. The average fractions of PEO cylinders and CdS/PEO spheres are also listed. In Figure 3B-1(c), more spherical CdS/PEO domains appear when 14 wt.-% CdS nanoparticles are incorporated. The average length of PEO cylinders shrinks to between 80 to 150 nm, with a diameter of ca. 15 nm, which is shorter and thinner than that of PEO cylinders in pure SEO. Figure 3B-1(d) shows that as the CdS content increases to 28 wt.-%, CdS-included PEO domains completely transform into a spherical morphology, as determined by AFM imaging, and TEM, where the majority of CdS-incorporated spherical PEO domains are observed to form arrays. The size of spherical CdS/PEO domains is ca. 40 to 50 nm, and the inter-sphere distance is ca. 70 nm. The CdS/PEO spherical morphology is confirmed by examining a cross-sectional image of the 28 wt.-% CdS/SEO thin film (ca. 100-nm thick), which has been immersed in water and sectioned in liquid nitrogen. Because the CdS/PEO domains are soluble in water, round holes appear in the cross-sectional SEM image of the 100-nm thick, 28 wt.-% CdS/SEO film, indicating that the shape of CdS/PEO domains are indeed spherical, not oriented cylinders perpendicular to the surface. Combining AFM, TEM and SEM results of the 28 wt.-% CdS/SEO film, the CdS clusters act as some kind of spherical site in the center of the CdS/PEO domains leading to a “spherical double-brushes”, with a CdS core, a first PEO corona covered by an outer PS corona which also forms the matrix into which the CdS/PEO spherical domains are embedded. The morphological transformation from cylindrical PEO into spherical CdS/PEO domains can be observed clearly when loading the surface-hydroxylated CdS. A control experiment with the same process to prepare thin film was carried out, in which only surfactant, mercaptoethanol, is added to SEO; no morphological change was observed to occur. The main cause of this morphological transformation might be due to a strong interaction between the hydroxyl groups on the surface of

CdS clusters and PEO domains.

The interaction between mercaptoethanol ligands on CdS and PEO blocks is attributed to dipole-dipole or hydrogen bonding interactions, which can be investigated by FTIR and NMR. Figure 3B-2 shows FTIR spectra of CdS/SEO thin films with various CdS content. As the CdS content increases, a broad peak in the free O-H stretching region at roughly 3450 cm^{-1} appears, which is attributed to hydroxyl groups on CdS and adsorbed moisture. Another small, but broad peak, generated by a hydrogen-bonding interaction between the hydroxyl groups on CdS and PEO, is observed at roughly 3250 cm^{-1}. It is not possible to identify the cause of the morphological transformation via this small peak, since spin-coated thin films are too thin to generate strong IR signals.

Figure 3B-3 shows ^{1}H NMR spectra for different amounts of CdS nanoparticles in SEO in ^{8}d-toluene; in curve (e), the spectrum of D_2SO_4 in SEO in d-toluene has been normalized using the PS peaks at 1.56 and 6.67 ppm as the standard and same solid content in ^{8}d-toluene. In Figure 3B-3(a), the case of pure SEO solution in d-toluene, broad peaks at ca. 1.56, 2.05 and 6.40-7.20 ppm all correspond to protons in the PS block, and the sharp peaks at ca. 2.08, 7.00, 7.01 and 7.09 ppm are all attributed to protons in d-toluene. The narrow peak at ca. 3.49 ppm is assigned to protons in the CH_2 group next to oxygen in the PEO block. The presence of CdS in the PEO block in curves (b)-(d), which are enlarged portions of the spectra of CdS/SEO, cause the CH_2O peak for PEO at 3.49 ppm to reduce in size; a broad new peak at 4.09 ppm emerges as the CdS content in PEO increases. To identify this new peak, a 2-D ^{13}C-^{1}H NMR experiment for 14 wt.-% CdS/SEO was performed. Figure 3B-3(f) displays this spectrum, which contains the broad new peak at ca. 4.09 ppm for the protons in CH_2O groups in PEO, in place of the original peak at 3.49 ppm for pure SEO. Moreover, the sum of the areas under the peaks at 3.49 and 4.09 ppm in each

CdS/SEO NMR spectrum is almost equal to the area of the peak at 3.49 ppm in the pure SEO spectrum. These two facts suggest that the broad new peak at 4.09 ppm is due to a shift of the peak at 3.49 ppm. In order to elucidate the cause, reversible heating and cooling experiments were carried out on the samples. Figure 3B-3(g) shows NMR spectra of 14 wt.-% CdS/SEO in ^{8}d-toluene at 21 and 60^{o}C. For 14 %wt CdS/SEO heated to 60^{o}C in ^{8}d-toluene solution, the shifted CH_2O peak for CdS/PEO disappears, and the integral peak area at 3.49 ppm in the curve taken at 60^{o}C is restored, as shown in curve (g). Hydrogen bonding between CdS clusters and PEO in CdS/SEO nanocomposites can explain this behavior, since hydrogen bonds are destroyed at elevated temperatures.[29] Moreover, curve (e) shows a similar shift for the CH_2O group in PEO after protonation by the addition of D_2SO_4 in pure SEO/d-toluene solution, which indicates that the shift of the CH_2O group in PEO may be due to hydrogen bonding. Therefore, the broad and shifted CH_2O peak indicates that CdS nanoparticles connect with the PEO block via strong intermolecular forces (i.e., hydrogen-bonding between the hydroxyl groups of CdS and the oxygen of PEO). This interaction changes the microenvironment around the CH_2O groups in PEO, resulting in the morphological transformation from cylindrical PEO domains to spherical CdS/PEO domains.

Hence, the morphological transformation brought on by the incorporation of mercaptoethanol-modified CdS nanoparticles can be explained by hydrogen bonding. In the composite CdS/SEO system, two types of hydrogen bonding are involved. The first, as demonstrated in NMR studies, occurs between the free hydroxyl groups on CdS and the oxygen of PEO, which results in the segregation of CdS in PEO, a change in the surface energy of CdS/PEO domains, and a morphological transformation from PEO cylinders to CdS/PEO spheres. The other interaction is due to mutual hydrogen bonding between surface-hydroxylated CdS nanoparticles,

which causes them to self-aggregate. Therefore, the PEO chains which surround the CdS clusters form CdS/PEO spheres, and CdS nanoparticles aggregate in PEO domains, as shown in scheme 3B-1. Comparisons between the percentage of shifted CH_2O protons in PEO (blue solid dots) and the percentage of CdS/SEO morphological spheres (white hollow squares) for various CdS content is presented in Table 3B-1 and Figure 3B-4. When the content of CdS is low (ca. 0-14 wt.-%), the percentages of both shifted CH_2O protons in PEO (ca. 0-62.3 %) and CdS/SEO spheres (ca. 3-67 %), which depend linearly on CdS content, show the same trace. This indicates that CdS is scarce in the PEO domains for low CdS content. For high CdS content (28 wt.-%), all CdS/PEO domains are spheres in the thin film morphology, but only 84.4 % of PEO chains connect to CdS, a result that is not linearly dependent on CdS content. This indicates that more CdS nanoparticles clump together instead of connecting to PEO chains when the CdS content is high (28 wt.-%), and the remaining 15.6 % exist as free ethylene oxide units present between CdS nanoparticles or are near the interface between PS and PEO domains.

3-4 Conclusions

In the case of CdS/LSEO thin films, the morphological transformation from PEO cylinders to spheres in thin films, due to the incorporation of CdS nanoparticles, is clearly observed in AFM, TEM and SEM images. The transformation is explained by hydrogen bonding interactions between surface-hydroxylated CdS and PEO, as demonstrated by NMR studies. Hydrogen bonding changes the chemical environment of PEO next to the CdS clusters. In the case of 28 %wt CdS/SEO thin films, the ordered arrangement of CdS clusters is fabricated via an SEO block copolymer template.

Moreover, we have provided a method to control the spatial position of CdS

nanoclusters using a specific interaction between surface ligands and one block of a self-assembled diblock copolymer template by first selectively dispersing these nanoparticles in one particular block of a diblock copolymer, in bulk, and then using solvent selectivity to sequester CdS nanoparticles in the block copolymer thin film. The inter-domain distance of the nanoclusters can be altered by changing the molecular weight of the other block of the diblock copolymer. Long-range order in CdS/LSEO thin films has been obtained using a patterned substrate. The incorporated nanoparticles retain their luminescence characteristics, as in the pure state. The CdS nanoparticles can be replaced by other nanoparticles or quantum dots, as long as proper surface ligands can be found.

References

1. F. S. Bates, *Science* **1991**, *251*, 898.
2. G. Reiter, G. Castelein, J.-U. Sommer, A. Rollele, T. Thurn-Albrecht, *Phys. Rev. Lett.* **2001**, *87*, 226101.
3. L. Li, Y. Serero, Michel H. J. Koch, Wim H. de Jeu, *Macromolecules* **2003**, *36*, 529.
4. S. Jiang, A. Gopfert, B. Abetz, *Macromolecules* **2003**, *36*, 6171.
5. L. Zhu, S. Z. D. Cheng, P. Huang, Q. Ge, R. P. Quirk, E. L. Thomas, Lotz, B. B. S. Hsiao, F. Yeh, L. Liu, *Advanced Materials* **2002**, *14*, 31.
6. R. A. Segalman, A. Hexemer, E. J. Kramer, *Phys. Rev. Lett.* **2003**, *91*, 196101.
7. S. Choi, K. M. Lee, C. D. Han, N. Sota, T. Hashimoto, *Macromolecules* **2003**, *36*, 793.
8. E. Buck, J. Fuhrmann, *Macromolecules* **2001**, *34*, 2172.
9. D. Sundrani, S. B. Darling, S. J. Sibener, *Nano Letters* **2004**, *4*, 273.
10. N. Rehse, A. Knoll, R. Magerle, G. Krausch, *Macromolecules* **2003**, *36*, 3261.

11. S. Forster, M. Antonietti, *Advanced Materials* **1998**, *10*, 195.
12. M. Lazzari, M. A. Lopez-Quintela, *Advanced Materials* **2003**, *19*, 1583.
13. C. Park, J. Yoon, E. L. Thomas, *Polymer* **2003**, *44*, 6725.
14. I. W. Hamley, *Nanotechnology* **2003**, *14*, R39.
15. M. R. Bockstaller, Y. Lapentnikov, S. Margel, E. L. Thomas, *J. Am. Chem. Soc.* **2003**, *125*, 5276.
16. (a) J. Y. Lee, R. B. Thompson, D. Jasnow, A. C. Balazs, *Macromolecules* **2002**, *35*, 4855; (b) J. Y. Lee, A. C. Balazs, R. B. Thompson, R. M. Hill, *Macromolecules* **2004**, *37*, 3536.
17. (a) S. W. Yeh, K. H. Wei, Y. S. Sun, U. S. Jeng, K. S. Liang, *Macromolecules* **2003**, *36*, 7903; (b) U. S. Jeng, Y. S. Sun, H. Y. Lee, C. H. Hsu, K. S. Liang, S. W. Yeh, K. H. Wei *Macromolecules* **2004**, *37*, 4617; (c) C. C. Weng, K. H. Wei, *Chem. Mater.* **2003**, *15*, 2936.
18. M. Haupt, S. Miller, R. Glass, M. Arnold, R. Sauer, K. Thonke, M. Moller, J. P. Spatz, *Advanced Materials* **2003**, *15*, 829.
19. J. I. Abes, R. E. Cohen, C. A. Ross, *Chem. Mater.* **2003**, *12*, 1125.
20. B. H. Sohn, J. M. Choi, S. Yoo, S. H. Yun, W. C. Zin, J. C. Jung, M. Kanehara, T. Hirata, T. Teranishi, *J. Am. Chem. Soc.* **2003**, *125*, 6368.
21. M. Park, C. Harrison, P. M. Chaikin, R. A. Register, D. H. Adamson, *Science* **1997**, *276*, 1401.
22. (a) K. Shin, K. A. Leach, J. T. Goldbach, D. H. Kim, J. Y. Jho, M. Tuominen, C. J. Hawker, T. P. Russell, *Nano Letters* **2002**, *2*, 933; (b) M. Bal, A. Ursache, M. Tuominen, J. T. Goldbach, T. P. Russell, *Appl. Phys. Lett.* **2002**, *81*, 3479. (c) Lin, Y.; Skaff, H.; Emrick, T.; Dinsmore, A. D.; Russell, T. P.; *Science* **2003**, *299*, 226.
23. J. Y. Cheng, C. A. Ross, V. Z.-H. Chan, E. L. Thomas, R. G. H. Lammertink, G. J. Vancso, *Advanced Materials* **2001**, *13*, 1174.

24. W. A. Lopes, H. M. Jaeger, *Nature,* **2001**, 414, 735.

25. M. J. Misner, H. Skaff, T. Emrick, T. P. Russell, *Advanced Materials* **2003**, *15*, 221.

26. D. E. Fogg, L. H. Radzilowski, R. Blanski, R. R. Schrock, E. L. Thomas, *Macromolecules* **1997**, *30*, 417.

27. S. W. Yeh, T. L. Wu, K. H. Wei, *Nano Letters* (submitted).

28. (a) J. G. C. Veinot, M. Ginzburg, W. J. Pietro, *Chem. Mater.* **1997**, *9*, 2117; (b) N. Herron, Y. Wang, H. Eckert, *J. Am. Chem. Soc.* **1990**, *112*, 1322.

29. M. J. Kunz, G. Hayn, R. Saf, W. H. Binder, *J. Polym. Sci. A: Polym. Chem.* **2004**, *42*, 661.

30. Cheng, J. Y.; Ross, C. A.; Thomas, E. L.; Smith, H. I.; Vancso, G. J.; *Advanced Materials* **2003**, *15*, 1599.

31. (a) Segalman, R. A.; Hexemer, A.; Kramer, E. J.; *Macromolecules* **2003**, *36*, 6831. (b) Segalman, R. A.; Hexemer, A.; Kramer, E. J.; *Phys. Rev. Lett.* **2003**, *91*, 196101.

32. Sundrani, D.; Darling, S. B.; Sibener, S. J.; *Nano Letters* **2004**, *4*, 273.

Scheme 3A-1 Fabrication of an ordered array of pre-synthesized nanoparticles using a block copolymer template by spin-coating a micellar solution. Nanoparticles are held in the cores of the micelles.

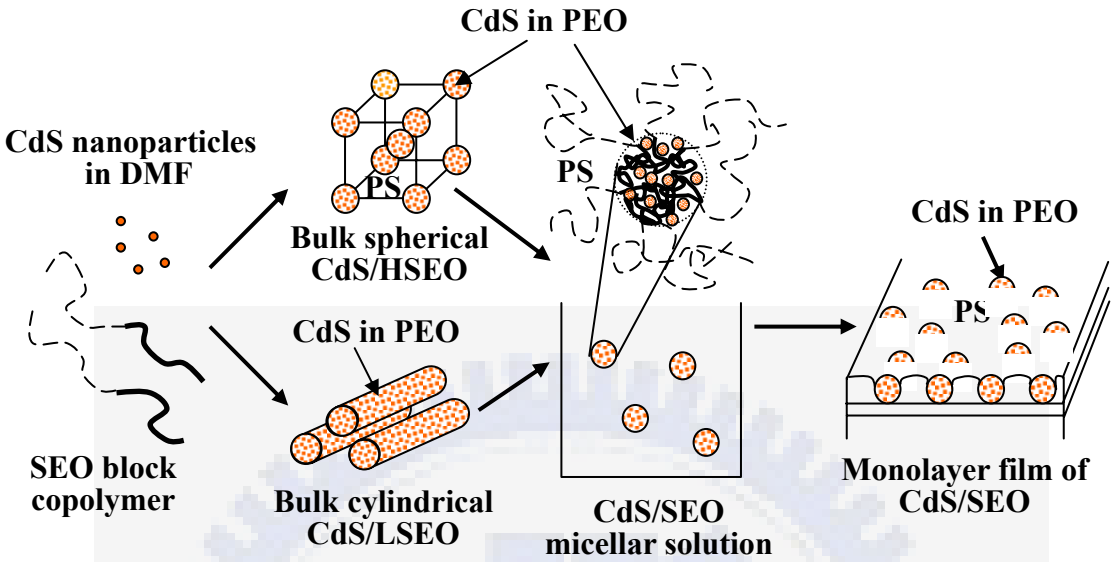

Scheme 3B-1 Morphological transformation of PEO cylinders into CdS/PEO spheres via hydrogen bonding interactions between surface-hydroxylated CdS and PEO.

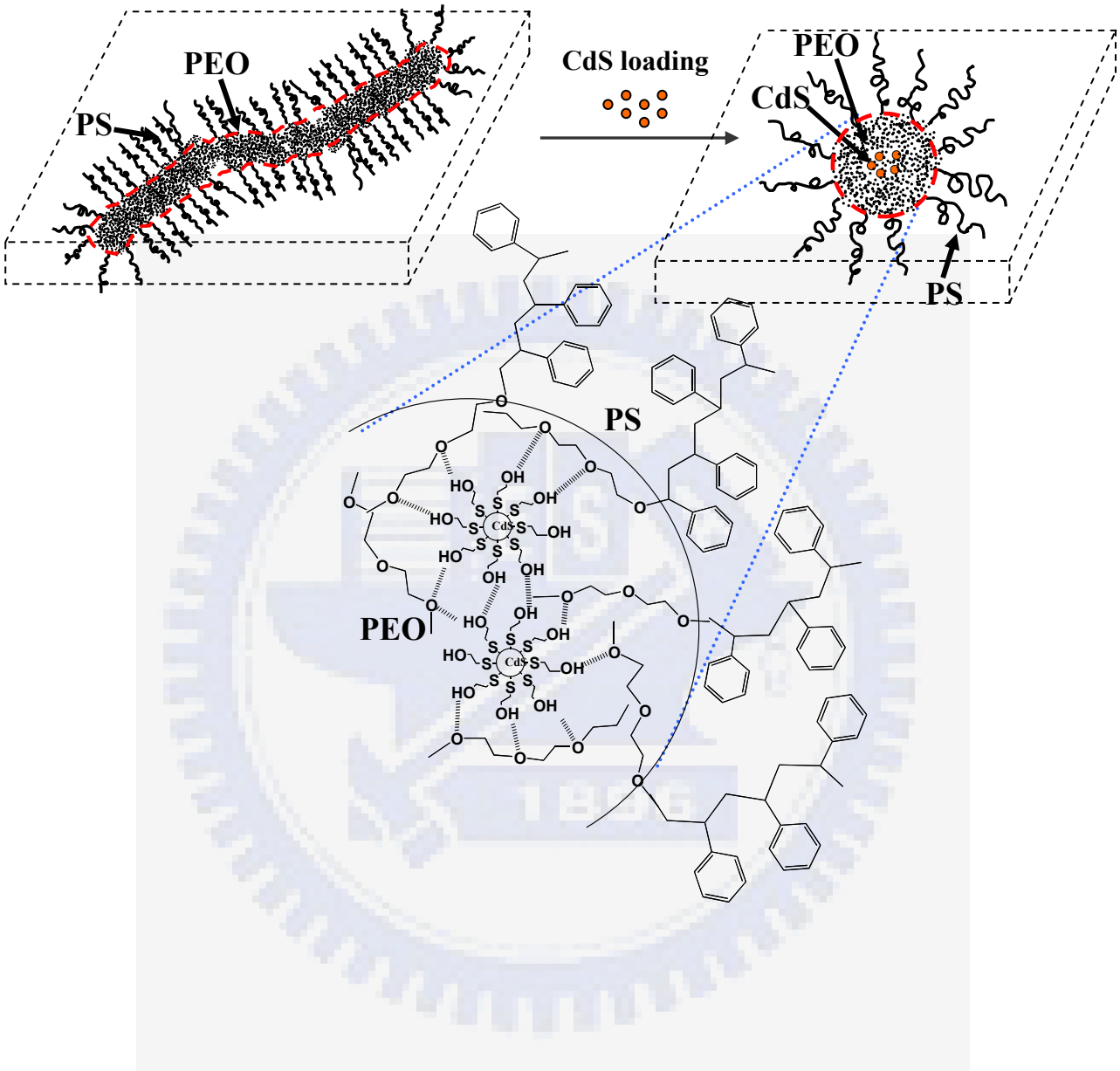

Table 3B-1 The percentage and average length of PEO cylinders, the percentage of CdS/PEO spheres, and the percentage of shifted CH_2O protons in PEO that appear in CdS/SEO thin films for various CdS content.

	Percentage of PEO cylinders [a]	Average length of PEO cylinders	Diameter of PEO cylinders	Percentage of CdS/PEO spheres [b]	Percentage of shifted protons of CH_2O in PEO [c]
Pure SEO	> 97 %	> 300 nm	18 nm	< 3 %	0 %
7 wt.-% CdS/SEO	71 %	200 ~ 300 nm	17 nm	29 %	29.1 %
14 wt.-% CdS/SEO	33 %	80-150 nm	15 nm	67 %	62.3 %
28 wt.-% CdS/SEO	0 %	------	------	100 %	84.4 %

[a, b] The percentage of PEO cylinders and CdS/PEO spheres is calculated by the ratio of $\frac{Area_{PEO}}{Area_{PEO} + Area_{CdS/PEO}}$ and $\frac{Area_{CdS/PEO}}{Area_{PEO} + Area_{CdS/PEO}}$ from AFM and TEM images.

[c] The percentage of shifted CH_2O protons in PEO is given from the integration of ^1H NMR curves.

Figure Captions:

Figure 3A-1 (a) AFM image of a CdS/HSEO thin film supported on a carbon-coated silicon wafer. (b) TEM image of CdS/HSEO thin film after removal from a carbon-coated silicon wafer with 1% HF solution.

Figure 3A-2 (a) AFM image of a CdS/LSEO thin film supported on a carbon-coated silicon wafer. (b) TEM image of a CdS/LSEO thin film after removal from carbon-coated silicon wafer with 1% HF solution.

Figure 3A-3 Phase contrast AFM images of a CdS/LSEO thin film on a patterned substrate with 400-nm wide grooves.

Figure 3A-4 Photoluminescence spectra of CdS in (a) DMF, thin films of (b) CdS/HSEO and (c) CdS/LSEO, and (d) pure LSEO.

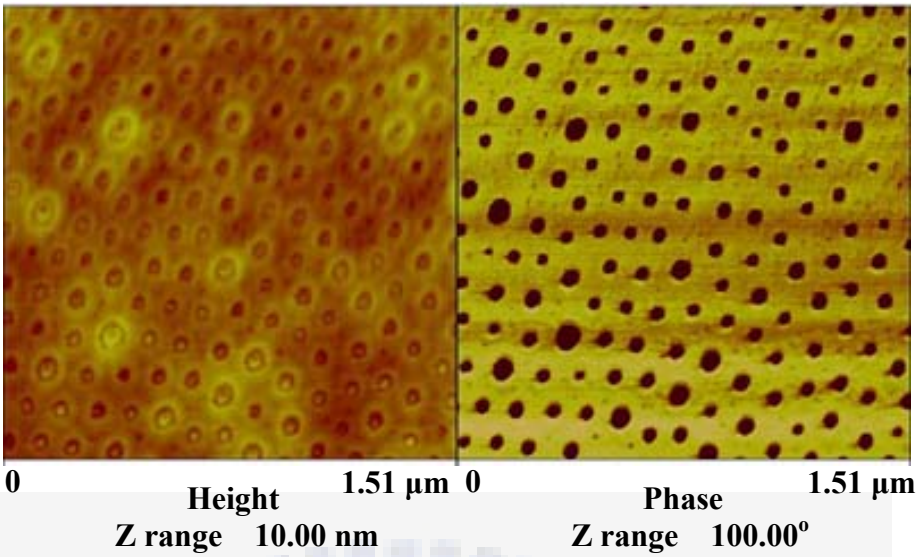

(a)

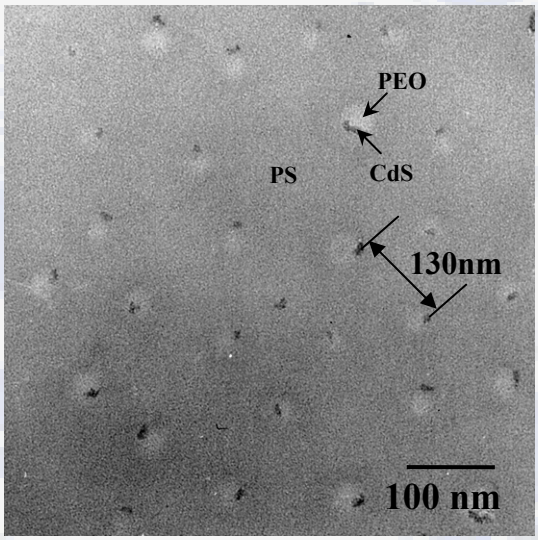

(b)

Figure 3A-1

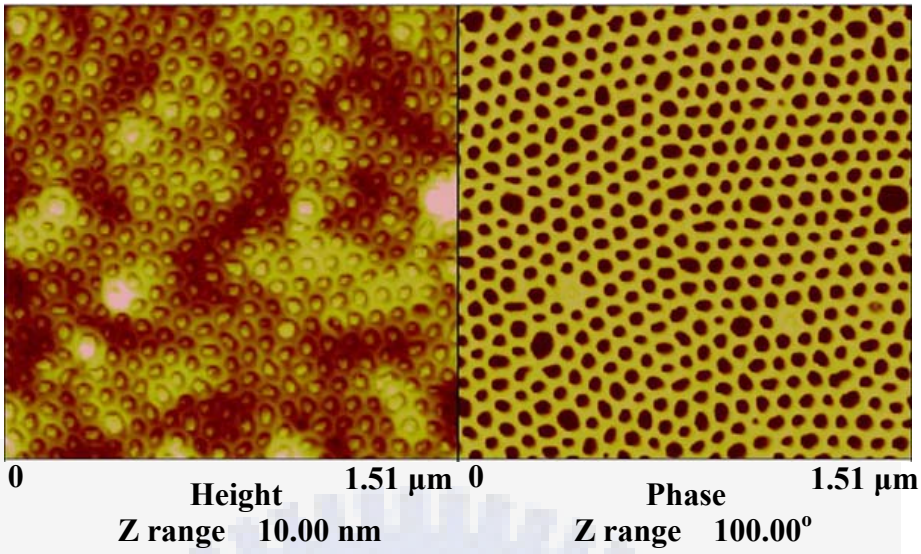

(a)

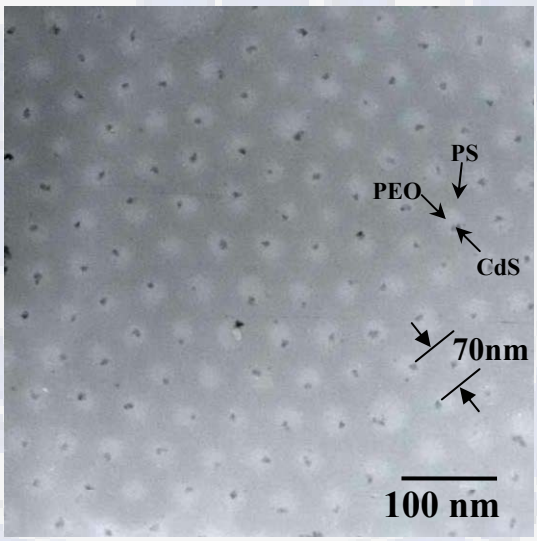

(b)

Figure 3A-2

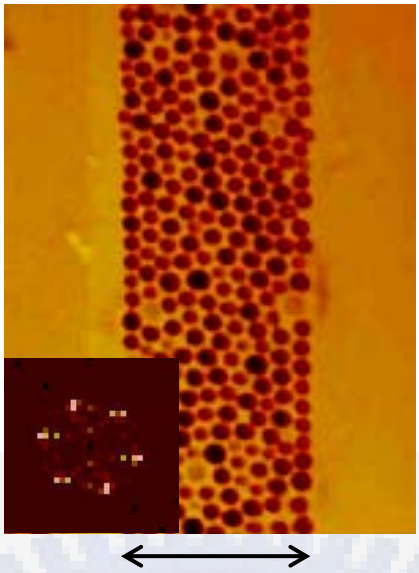

Figure 3A-3

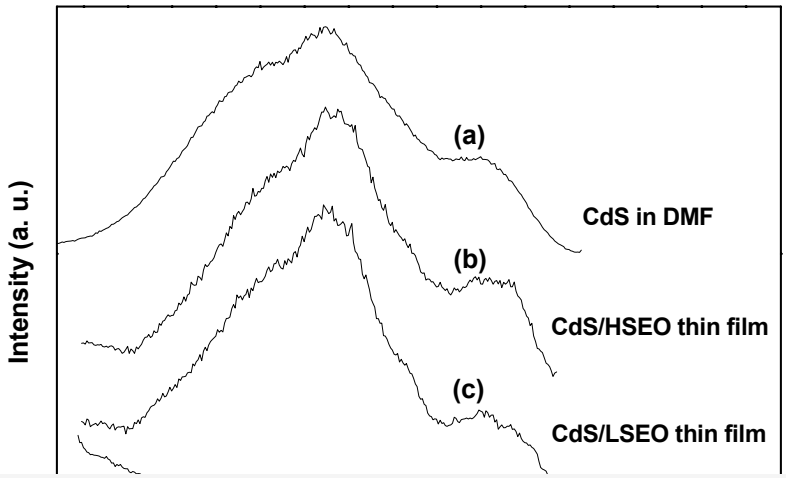
Intensity (a. u.)
(a)
CdS in DMF
(b)
CdS/HSEO thin film
(c)
CdS/LSEO thin film

Figure 3A-4

Figure Captions

Figure 3B-1. Phase contrast AFM images and TEM images of 40-nm-thick CdS/SEO thin films with (a) 0, (b) 7, (c) 14 and (d) 28 wt.-% CdS content after spin-coating onto carbon-coated silicon wafers. Figure 1(e). The SEM cross-sectional image of 28 wt.-% CdS nanoparticles in SEO thin film.

Figure 3B-2. ^{1}H NMR spectra of (a) 0, (b) 7, (c) 14 and (d) 28 wt.-% CdS/SEO and (e) D_2SO_4 in SEO in d-toluene after normalization. Figure 3A-3(f). A 2-D ^{13}C-^{1}H NMR spectrum of 14 wt.-% CdS/SEO. Figure 3A-3(g). NMR spectra of 14 wt.-% CdS/SEO at different temperatures (21 and 60^{o}C).

Figure 3B-3. The comparisons between the percentage of shifted CH_2O protons in PEO (blue solid dots) and the percentage of CdS/SEO morphological spheres (white hollow squares) for various CdS content

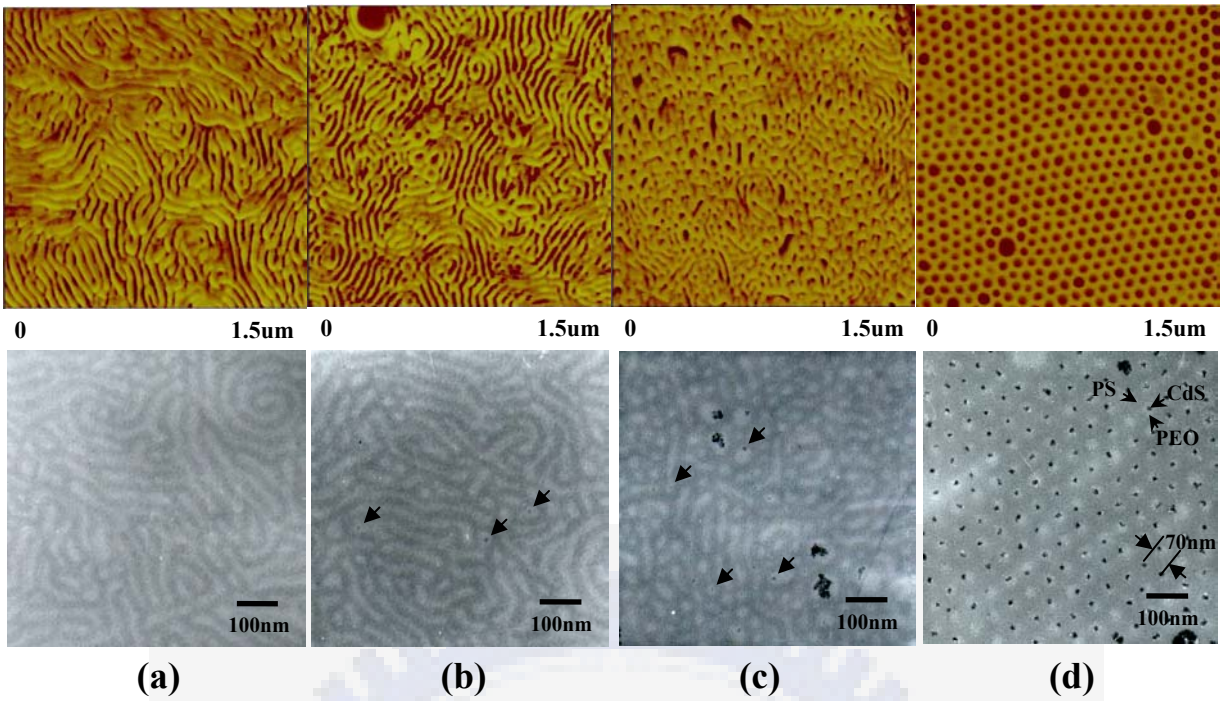
0
1.5um
0
1.5um
0
1.5um
0
1.5um
100nm
100nm
100nm
PS
CdS
PEO
70nm
100nm
(a)
(b)
(c)
(d)

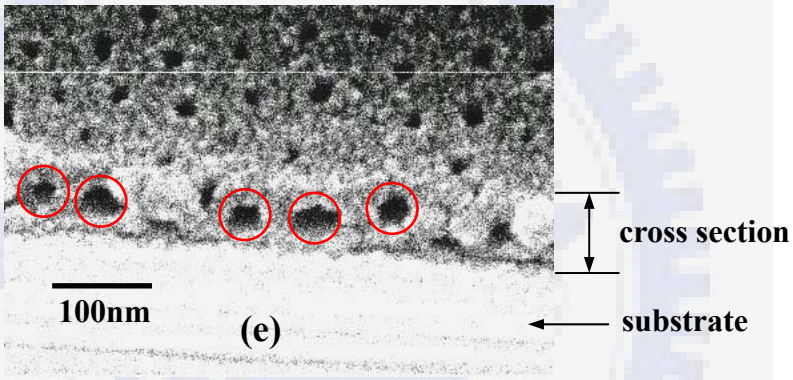
cross section
100nm
(e)
substrate

Figure 3B-1

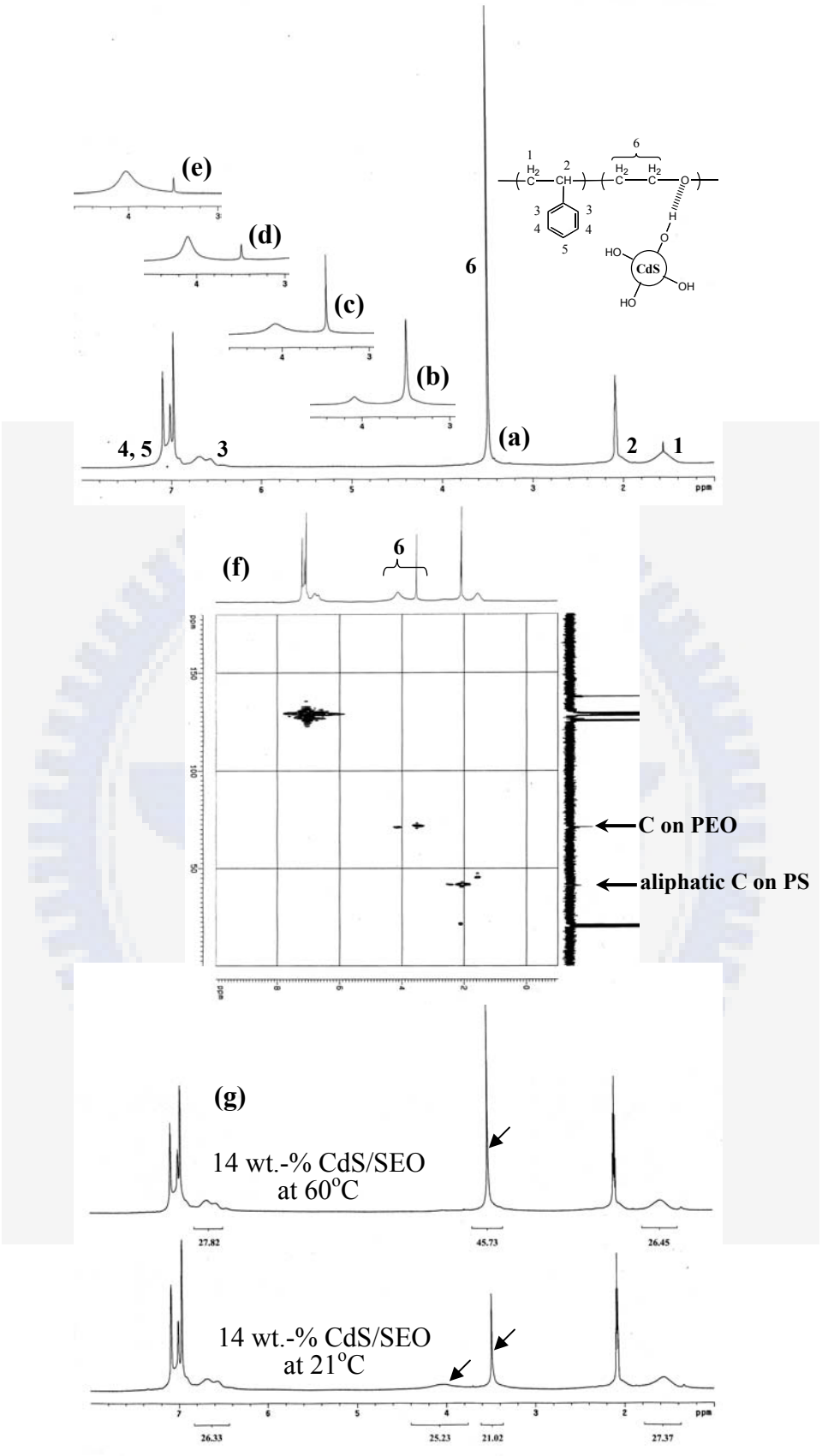
(e)
(d)
(c)
(b)
(a)
6
4, 5
3
2
1
ppm
CdS
(f)
6
C on PEO
aliphatic C on PS
(g)
14 wt.-% CdS/SEO
at 60°C
27.82
45.73
26.45
14 wt.-% CdS/SEO
at 21°C
26.33
25.23
21.02
27.37

Figure 3B-2

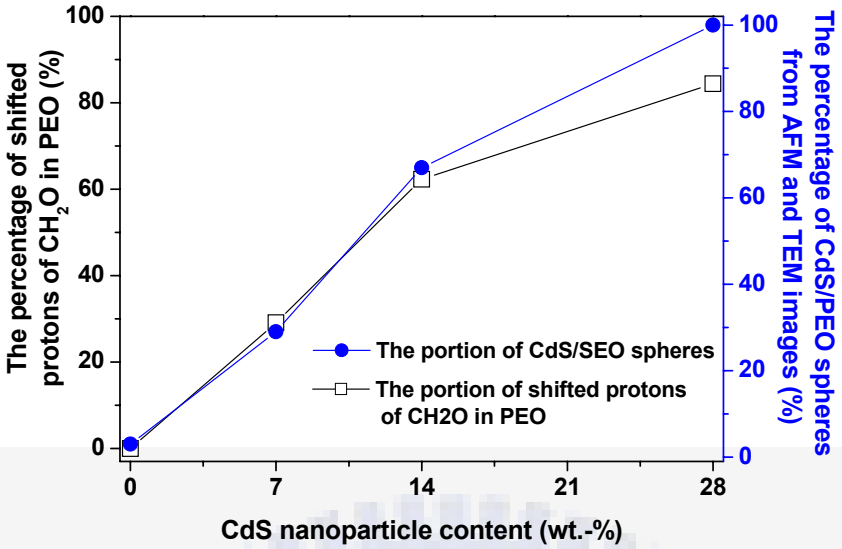
The percentage of shifted protons of CH_2O in PEO (%)
The percentage of CdS/PEO spheres from AFM and TEM images (%)
CdS nanoparticle content (wt.-%)
The portion of CdS/SEO spheres
The portion of shifted protons of CH2O in PEO
0
20
40
60
80
100
0
7
14
21
28

Figure 3B-3

Chapter 4: Effects of CdS in S4VP Bulk Samples

4-1 Introduction

Block copolymers are versatile platform materials because they can self-assemble into various nanostructures with period thicknesses between 10 to 100 nm, under the appropriate compositions and conditions, owing to microphase separation between incompatible blocks.[1-10] Hence, self-assembled block copolymers in bulk and thin film forms can, therefore, be used as templates for bringing nanoparticles into ordered nanostructures as demonstrated in several studies.[11-22] For examples, a segregation of gold nanoparticles in a polystyrene-b-poly(ethylene/propylene) block copolymer was reported.[15] Other metal nanoparticles formed by in-situ reduction in the microdomain of a block copolymer were also reported.[16] Moreover, using a poly(styrene-b-4-vinylpyridine) (S4VP) micellar solution, ordered Au clusters,[17] Co and Fe arrays,[18] and self-assembly of both Au and Fe_2O_3 nanoparticles[19] have been obtained. Au, Ag[20] and magnetic Co[21] nanowires can also be produced using a PS-b-PMMA block copolymer template. The morphology of block copolymers involving nanoparticles has been predicted by a theoretical study by Balazs'group.[24] Additionally, for semiconductor nanoparticles, the selective sequestration of pre-synthesized surface-modified CdS or TiO_2 nanoparticles into one block of poly(styrene-b-ethylene oxide) (SEO)[25a] or poly(styrene-b-methyl methacrylate) (SMMA)[25c] has been performed, respectively. The morphological transformation of bulk CdS/SEO with a higher molecular weight of SEO (PS/PEO = 125k/16.1k, volume fraction of PEO = 0.11) is also observed. The binding of nanoparticles exclusively to the PEO chains results in CdS/PEO composite microdomain with greatly enhanced thermal stability.[25b] Moreover, the sequestered CdS clusters in the

PEO domains of SEO block copolymer thin films (PS/PEO = 19k/12.6k, volume fraction of PEO = 0.3) induce the morphological transformation of PEO microdomain to spheres from cylinders by the presence of hydrogen bonds.[25d]

In this article, we report a morphological transformation of S4VP to a lamellar structure from a hexangonally-packed cylinder structure due to the sequestered CdS nanoparticles in P4VP block. The binding of CdS nanoparticles into P4VP domains is caused by hydrogen bonds between them as evidenced by ^{1}H nuclear magnetic resonance (NMR) spectra, and is supported by glass transition temperatures measurements. Moreover, this morphological transformation induced by CdS nanoparticles is consistent with the phase diagram predicted by a theoretical study of the copolymer/particle mixture system.

4-2 Methods and Analysis

The surfactant, containing a chemically-active carboxylic acid groups on surface, makes CdS hydrophilic, and CdS nanoparticles were dispersed in N, N-dimethylforamide (DMF). Subsequently, CdS/DMF was added to a previously prepared S4VP/DMF solution under stirring. This mixture was dried slowly under vacuum at 323 K and then maintained at 413 K for 24 hours, after which CdS/S4VP nanocomposites were obtained. Thermal gravimetric analysis was used to ensure no residual DMF solvent was present. Here, two CdS content, 7% and 28% CdS by weight fraction respect to P4VP block, were prepared. ^{1}H NMR ($CDCl_3$): δ = 6.50 (m, H_a), 7.05 (s, H_b), 8.30 (s, H_c).

Small-angle X-ray scattering experiments were performed on wiggler beamline BL-17B1 at the National Synchrotron Radiation Research Center, Taiwan. Transmission electron microscopy was performed on a Hitachi H-600 instrument operating at 100kV; ultrathin sections of CdS/S4VP nanocomposites for TEM

studies were microtomed with Leica Ultracut Uct equipped with a diamond knife and subsequently deposited on copper grids. The microtomed thin films, corresponding to the section of CdS/S4VP nanocomposites, were also been observed by atomic force microscopy (AFM). AFM measurements were performed with a Digital Nanoscope IIIa. ^{1}H NMR spectra for hydrogen bonding studies were recorded on a Varian Unity-300 MHz NMR spectrometer by using ^{8}d-toluene as the solvent. The glass transition temperatures (Tg) of the samples were obtained from a Dupont DSC 2910 instrument at a heating rate of 10℃/min.

4-3 Results and Discussions

Figure 4-1 shows TEM (left side) and phase contrast AFM (right side) images of S4VP containing different amount of CdS nanoparticles. In the TEM image of S4VP (Figure 4-1(a)), the dark region, due to staining by iodine, is the P4VP domain, and the light region is the PS domain. In the TEM image, the round and cylindrical shapes of P4VP domains correspond to the cross section and the side view of the cylindrical structure of P4VP domains, respectively. The pure S4VP has a hexagonally-packed cylindrical (HEX) structure that is constituted by 23nm-diameter P4VP cylinders with an inter-cylinder distance of 52nm. This cylindrical morphology was also displayed in the phase-contrast image of microtomed S4VP thin films with atomic force microscopy. In the AFM image of S4VP, the light round is the cross section, and cylindrical part is the oblique cross section of cylindrical P4VP phase, and the dark part is PS domain. In the presence of 7% CdS nanoparticles, as shown in Figures 4-1(b), the dark color phase in the TEM image represents the P4VP/CdS composite phase, because of the higher electron density of cadmium. CdS nanoparticles in this case are apparently segregated selectively in P4VP domains, by the dipole-dipole interactions between

the carboxylic acid groups of mercaptoacetic acid on CdS and the P4VP chains. The morphology of the CdS/S4VP, however, becomes a lamellar structure that consists of alternating 28nm thick PS and 12nm thick CdS/P4VP lamellae. The AFM image of CdS/S4VP thin films also shows a consistent topology with the TEM morphology. The volume ratio of CdS/P4VP domain in the lamellar CdS/S4VP composite is about 0.3 as determined by the lamellae thicknesses, which is also matched with that calculated by molecular weight. In the case of 28% CdS/S4VP, CdS aggregates cause a number of defects in the lamellar structure, and the long-range order of the lamellar structure was destroyed, as shown in the TEM and AFM images in Figure 4-1(c).

The morphology of pure S4VP block copolymers and S4VP containing segregated CdS nanoparticles can be further examined in one-dimension small-angle X-ray scattering (SAXS) study. Figure 4-2 shows SAXS curves of pure S4VP and CdS/S4VP by synchrotron radiation. For pure S4VP, structure-factor peaks appear at Q = 0.0137, 0.0234, 0.0357 and 0.0408 $Å^{-1}$, corresponding to a ratio of $1:3^{1/2}:7^{1/2}:9^{1/2}$. This ratio indicates a typical scattering by a hexagonally-packed cylinders (HEX) structure. The inter-cylinder distance (*D*) was determined to be 53 nm by equation (1).

$$D = \left(\frac{3}{2}\right)^{1/2} * d_{100} \qquad (1)$$

where $d_{110}=2\pi/Q_{110}$ and $Q_{110}= 0.137\ nm^{-1}$. In the case of S4VP containing 7% CdS in P4VP domains, the scattering peaks are located at Q = 0.0137, 0.0271 and 0.0395 $Å^{-1}$, corresponding to a ratio of 1:2:3. This ratio implies that the scattering is caused by a lamellar structure. The inter-lamella distance is 45.8 nm, as determined from equation (2).

$$D = d_{100} \qquad (2)$$

where $d_{100}=2\pi/Q_{100}$ and $Q_{100}= 0.137\ nm^{-1}$. The SAXS results are consistent with the TEM results, confirming that the HEX structure of pure S4VP has been induced to a lamellar morphology in the presence of CdS nanoparticles. In the case of 28% CdS/S4VP, however, no scattering peaks were detected, indicating that the long-range ordered lamellar structure of S4VP is destroyed. The morphological transformation and the structural destruction of S4VP block copolymers with various CdS content is illustrated in scheme 4-1.

It should be noted that the amounts of CdS nanoparticles, 7% and 28% by weight with respect to the P4VP block, are about 1.35% and 5.4% by volume, which are not enough to swell the P4VP phase into the region of a lamellar structure that should have a volume fraction of between 0.4 and 0.6. The morphological transformation from cylindrical pure S4VP to lamellar CdS/S4VP can be manifested by strong interaction force such as hydrogen bond, between the carboxylic acid of CdS nanoparticles and poly(4-vinylpyridine) chains. Figure 4-3 shows the enlarged portions of ^{1}H NMR spectra of pure S4VP and CdS/S4VP with 7 % and 28% CdS in P4VP. In Figure 4-3, peak **b** at 7.05 ppm corresponds to the protons of benzene rings in the PS block ($\mathbf{H_b}$), and they are affected by the presence of CdS nanoparticles in P4VP domains. The relative intensity of peak **c** and **a** at 8.30 ppm and 6.50 ppm, however, decreases with the increasing amount of CdS nanoparticles. The peak **c** are associated with the protons in pyridine rings ($\mathbf{H_c}$), and the peak **a** is due to protons in both the pyridine and benzene rings ($\mathbf{H_a}$). In the presence of CdS nanoparticles, the ratio of peak **c** to peak **b** is reduced to 0.12 in the 7% CdS/S4VP case from 0.23 in the pure S4VP case. The peak **c** disappears in the case of 28% CdS/S4VP. The ratio of peak **a** to peak **b** is reduced to 0.85 in 7% CdS/S4VP and 0.68 in the 28% CdS/S4VP case from 0.95 in pure S4VP. The reduction in the peak intensity due to hydrogen atoms, $\mathbf{H_a}$ and $\mathbf{H_c}$, in pyridine rings indicates the loss

of mobility in pyridine rings because of hydrogen bonds between carboxylic acid groups on the surface of CdS nanoparticles and P4VP chains, which is similar to the previous study.[27]

Further evidence of a loss of mobility of P4VP chains when binding CdS nanoparticles can be found in the glass transition temperature of P4VP chains (Tg_{P4VP}). Figure 4-4 shows the DSC results of pure S4VP and CdS/S4VP with 7% CdS and 28% CdS in P4VP. In pure S4VP, glass transition temperature of PS (Tg_{PS}) and P4VP (Tg_{P4VP}) chains appear clearly at 104°C and 147°C, respectively. In the presence of 7% and 28% CdS in P4VP, however, only Tg_{PS} is observed, indicating that the mobility of P4VP chains is retarded by CdS nanoparticles.

A theoretical study on diblock copolymer/nanoparticles have been carried out recently by Balazs' group, and they generated phase diagrams to predict the structural transition of a A-B block copolymer/particle mixture system by the variations in the particle interaction.[24c] Assuming that the P4VP blocks are unperturbed Gaussian chains, the radius of gyration of P4VP chains was estimated to be 45.9 Å by $R_g=(1/6)^{1/2}aN^{1/2}$ where a is statistic segment length (a_{P4VP}=7.97 Å)[28] and N degree of polymerization (N_{P4VP}=199). Concerning the phase diagram in Figure 4-5, which is taken and modified from Ref. 24(c), A, B, P and χ correspond respectively to PS, P4VP, CdS and the enthalpic interaction in our system, respectively, and the f_A stands for the fraction of PS segments in a S4VP chain (f_A = 0.7 in this case). The S4VP diblock copolymer was under strong segregation limit ($\chi_{AB}N > 100$).[24(c), 29] The size of CdS particle (R_p~18.4 Å) can be described as $R \approx 0.4R_g$. In pure S4VP system, as shown in Figure 4-5, the morphology is determined only by the volume fraction, and an HEX morphology were obtained. In the presence of 7% CdS, however, the value of χ_{BP} is negative,

due to the presence of hydrogen bonding between P4VP and CdS nanoparticles. In the phase diagram of block copolymer/particle mixture system, the negative χ_{BP} causes the morphological transformation from a cylindrical structure to a lamellar structure, which is consistent with our experimental results. As CdS content is increased to 28%, the deformation of lamellae structure and the loss of the long-range ordering can be explained by the fact that large amount of CdS nanoparticles fill up a large fraction of free spacing in P4VP domains and segregate irregularly. Balazs et al. also suggested that self-assembled structures could be either stable or metastable, depending on the volume faction and particle size.[24(a)]

4-4 Conclusions

In conclusion, CdS nanoparticles segregated P4VP domains of S4VP block copolymers by the hydrogen bonds induces the morphological change from hexagonally-packed P4VP cylinders to lamellar structure of CdS/S4VP composites. The experimental data of the morphological transformation of CdS/S4VP composites is consistent with the prediction of the nanoparticles/block copolymers system in theory.

Acknowledgment

The authors would like to acknowledge the National Science Council and the US Air Force Office of Scientific Research for funding this work through NSC 91-2120-M-009-001 and AOARD-03-4018, respectively.

References

1. (a) Bates, F. S.; Fredrickson, G. H. *Annu. Rev. Phys. Chem.* **1990**, *41*, 525. (b)

Bates, F. S. *Science* **1991**, *251*, 898.

2. (a) Reiter, G.; Castelein, G.; Sommer, J.-U.; Rollele, A.; Thurn-Albrecht, T. *Phys. Rev. Lett.* **2001**, *87*, 226101. (b) Rottele, A.; Thurn-Albrecht, T.; Sommer, J. U.; Reiter, G. *Macromolecules* **2003**, *36*, 1257.
3. Li, L.; Serero, Y.; Koch, M. H. J.; de Jeu, W. H. *Macromolecules* **2003**, *36*, 529.
4. Jiang, S.; Gopfert, A.; Abetz, B. *Macromolecules* **2003**, *36*, 6171.
5. (a) Zhu, L.; Huang, P.; Chen, W. Y.; Weng, X.; Cheng, S. Z. D.; Ge, Q.; Quirk, R. P.; Senador, T.; Shaw, M. T.; Thomas, E. L.; Lotz, B.; Hsiao, B. S.; Yeh, F.; Liu, L. *Macromolecules* **2003**, *36*, 3180. (b) Zhu, L.; Cheng, S. Z. D.; Huang, P.; Ge, Q.; Quirk, R. P.; Thomas, E. L.; Lotz, B.; Hsiao, B. S.; Yeh, F.; Liu, L. *Advanced Materials* **2002**, *14*, 31.
6. (a) Segalman, R. A.; Hexemer, A.; Kramer, E. J. *Macromolecules* **2003**, *36*, 6831. (b) Segalman, R. A.; Hexemer, A.; Kramer, E. J. *Phys. Rev. Lett.* **2003**, *91*, 196101.
7. (a) Choi, S.; Lee, K. M.; Han, C. D.; Sota, N.; Hashimoto, T. *Macromolecules* **2003**, *36*, 793. (b) Chen, H. L.; Hsiao, S. C.; Lin, T. L.; Yamauchi, K.; Hasegawa, H.; Hashimoto, T. *Macromolecules* **2001**, *34*, 671.
8. (a) Buck, E.; Fuhrmann, J. *Macromolecules* **2001**, *34*, 2172. (b) Nick, L.; Lippitz, A.; Unger, W.; Kindermann, A.; Fuhrmann, J. *Langmuir* **1995**, *11*, 1912.
9. Sundrani, D.; Darling, S. B.; Sibener, S. J. *Nano Letters* **2004**, *4*, 273.
10. (a) Knoll, A.; Horvat, A.; Lyakhova, K. S.; Krausch, G.; Sevink, G. J. A.; Zvelindovsky, A. V.; Magerle, R. *Phys. Rev. Lett.* **2002**, *89*, 35501. (b) Rehse, N.; Knoll, A.; Magerle, R.; Krausch, G. *Macromolecules* **2003**, *36*, 3261.
11. (a) Forster, S.; Antonietti, M. *Advanced Materials* **1998**, *10*, 195; [11b]

Chernyshov, D. M.; Bronstein, L. M.; Borner, H.; Berton, B.; Antonietti, M. *Chem. Mater.* **2000**, *12,* 114.

12. Lazzari, M.; Lopez-Quintela, M. A. *Advanced Materials* **2003**, *19*, 1583.
13. Park, C.; Yoon, J.; Thomas, E. L. *Polymer* **2003**, *44*, 6725.
14. Hamley, I. W. *Nanotechnology* **2003**, *14*, R39.
15. (a) Bockstaller, M. R.; Lapentnikov, Y.; Margel, S.; Thomas, E. L. *J. Am. Chem. Soc.* **2003**, *125*, 5276. (b) Bockstaller, M.; Kolb, R.; Thomas, E. L. *Advanced Materials* **2001**, *13*, 1783.
16. (a) Ribbe, A. E.; Okumura, A.; Matsushige, K.; Hashimoto, T. *Macromolecules* **2001**, *34*, 8239. (b) Hashimoto, T.; Harada, M.; Sakamoto, N. *Macromolecules* **1999**, *32,* 6867.
17. (a) Haupt, M.; Miller, S.; Glass, R.; Arnold, M.; Sauer, R.; Thonke, K.; Moller, M.; Spatz, J. P. *Advanced Materials* **2003**, *15*, 829. (b) Spatz, J. P.; Herzog, T.; Mobmer, S.; Ziemann, P.; Moller, M. *Advanced Materials* **1999**, *11*, 149.
18. (a) Abes, J. I.; Cohen, R. E.; Ross, C. A. *Chem. Mater.* **2003**, *12*, 1125. (b) Boontongkong, Y.; Cohen, R. E. *Macromolecules* **2002**, *35*, 3647.
19. Sohn, B. H.; Choi, J. M.; Yoo, S.; Yun, S. H.; Zin, W. C.; Jung, J. C.; Kanehara, M.; Hirata, T.; Teranishi, T. *J. Am. Chem. Soc.* **2003**, *125*, 6368.
20. (a) Lopes, W. A.; Jaeger, H. M. *Nature,* **2001**, 414, 735. (b) Lopes, W. A.; *Phys. Rev. E* **2002**, *65*, 031606.
21. Bal, M.; Ursache, A.; Tuominen, M.; Goldbach, J. T.; Russell, T. P. *Appl. Phys. Lett.* **2002**, *81*, 3479.
22. (a) Cheng, J. Y.; Ross, C. A.; Chan, V. Z.-H.; Thomas, E. L.; Lammertink, R. G. H.; Vancso, G. J. *Advanced Materials* **2001**, *13*, 1174. (b) Cheng, J. Y.; Ross, C. A.; Thomas, E. L.; Smith, H. I.; Vancso, G. J. *Advanced Materials* **2003**, *15*, 1599.

23. Fogg, D. E.; Radzilowski, L. H.; Blanski, R.; Schrock, R. R.; Thomas, E. L. *Macromolecules* **1997**, *30*, 417.

24. (a) Huh, J.; Ginzburg, V. V.; Balazs, A. C. *Macromolecules* **2000**, *33*, 8085. (b)Thompson, R. B.; Ginzburg, V. V.; Matsen, M. W.; Balazs, A. C. *Science* **2001**, *292*, 2469. (c) Lee, J. Y.; Thompson, R. B.; Jasnow, D.; Balazs, A. C. *Macromolecules* **2002**, *35*, 4855.

25. (a) Yeh, S. W.; Wei, K. H.; Sun, Y. S.; Jeng, U. S.; Liang, K. S. *Macromolecules* **2003**, *36*, 7903. (b) Jeng, U. S.; Sun, Y. S.; Lee, H. Y.; Hsu, C. H.; Liang, K. S. *Macromolecules* **2004**, *37*, 4617. (c) Weng, C. C.; Wei, K. H. *Chem. Mater.* **2003**, *15*, 2936. (d) Yeh, S.W.; Chang, Y. T.; Chou, C. H.; Wei, K. H. *Macromolecular Rapid Communications* **2004**, *25*, 1679.

26. (a) Veinot, J. G. C.; Ginzburg, M.; Pietro, W. J. *Chem. Mater.* **1997**, *9*, 2117. (b) Herron, N.; Wang, Y.; Eckert, H. *J. Am. Chem. Soc.* **1990**, *112*, 1322.

27. (a) Chen, D.; Peng, H.; Jiang, M. *Macromolecules* **2003**, *36*, 2576. (b) Peng, H.; Chen, D.; Jiang, M. *J. Phys. Chem. B* **2003**, *107*, 12461. (c) Yao, X.; Chen, D.; Jiang, M. *J. Phys. Chem. B* **2004**, *108*, 5225.

28. Bolline C.; Stone, V. W.; Carlier,V.; Jonas, A. M. *Macromolecules*, **1999**, 32, 4718.

29. (a) Polushkin, E.; Albertda van Ekenstrin, G. O. R.; Knaapila, M.; Ruokolainen, J.; Torkkeli, M.; Serimaa, R.; Bras, W.; Dolbnya, I.; Ikkala, O.; ten Brink, G. *Macromolecules*, **2001**, 34, 4917. (b) Clarke, C. J.; Eisenberg, A.; Nguyen, D.; Schwarz, S. A.; Strzhemechny, Y.; Sauer, B. B.; *Macromolecules*, **1997**, 30, 4184.

Scheme 4-1 Hydrogen bonding induces the morphological transformation from a HEX structure of pure S4VP block copolymers to lamellar CdS/S4VP composites with selective segregation of CdS nanoparticles in P4VP phase. The overloading of CdS nanoparticles in P4VP domains causes a curvature of CdS/P4VP lamellar domains and a structural destruction due to the CdS aggregates

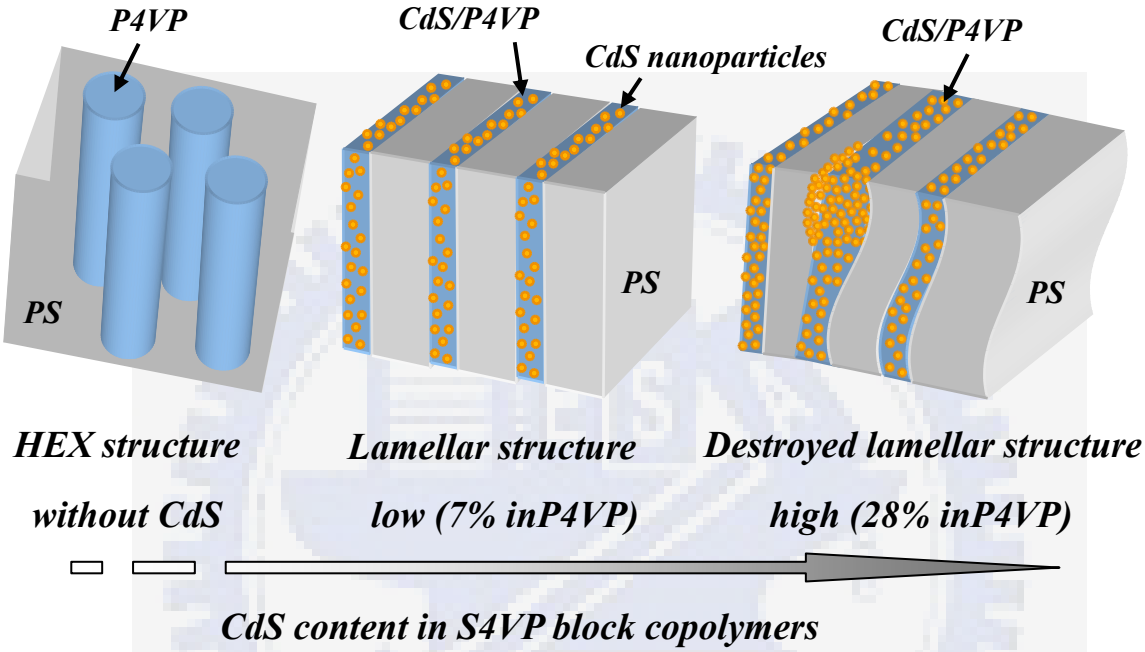

Figure Captions:

Figure 4-1. Transmission electron microscopy (left side) and phase contrast atomic force microscopy (right side) images of bulk pure S4VP and S4VP containing 7% and 28% CdS particles by weight.

Figure 4-2. Small-angle X-ray scattering curves of pure S4VP and S4VP containing 7% and 28% CdS nanoparticles.

Figure 4-3. ^{1}H NMR spectra of pure S4VP and S4VP containing 7% and 28% CdS nanoparticles by weight fraction, which respect to P4VP block.

Figure 4-4. The glass transition temperature of PS and P4VP domains of pure S4VP and S4VP containing 7% and 28% CdS nanoparticles, which are determined by DSC.

Figure 4-5 Phase diagram of the morphological transformation from a HEX structure of pure S4VP block copolymers to lamellar structure with selective segregation of CdS nanoparticles in P4VP phase. The diagram was modified from Figure 1(a) in ref. 24(c) by Balazs et al.

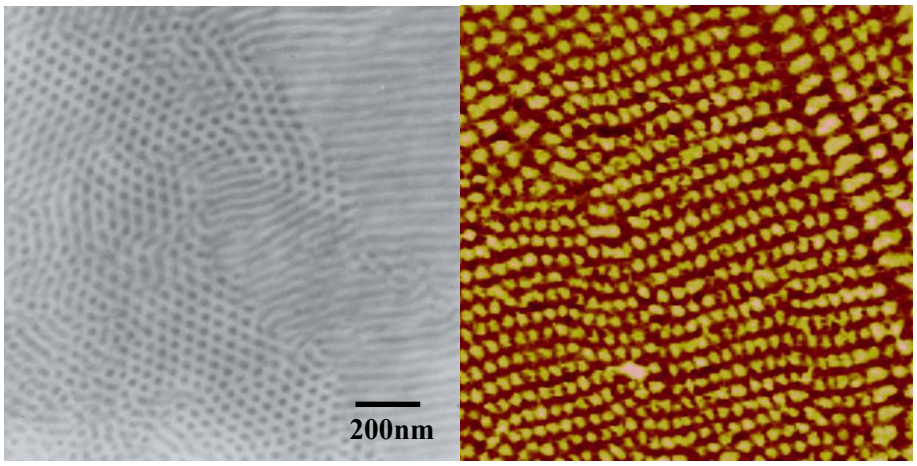

(a)

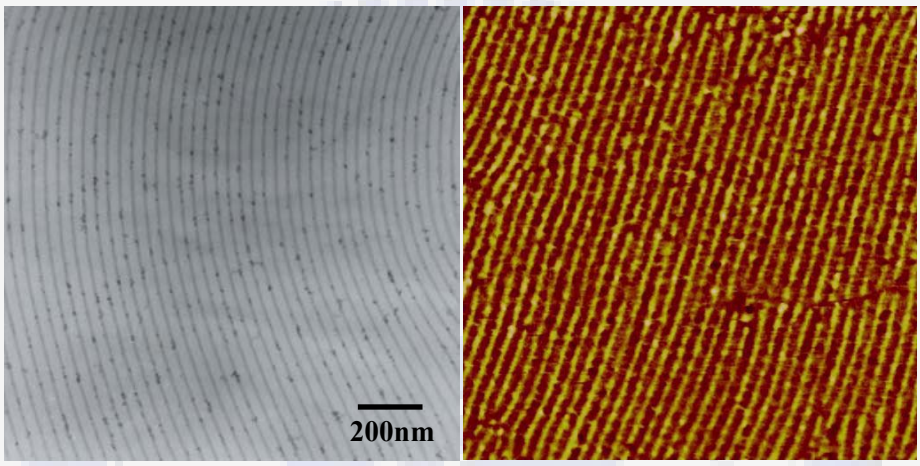

(b)

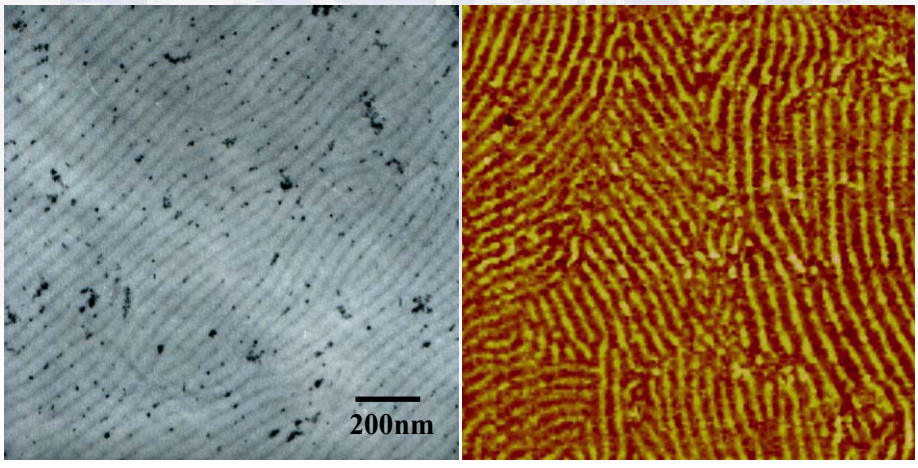

(c)

Figure 4-1

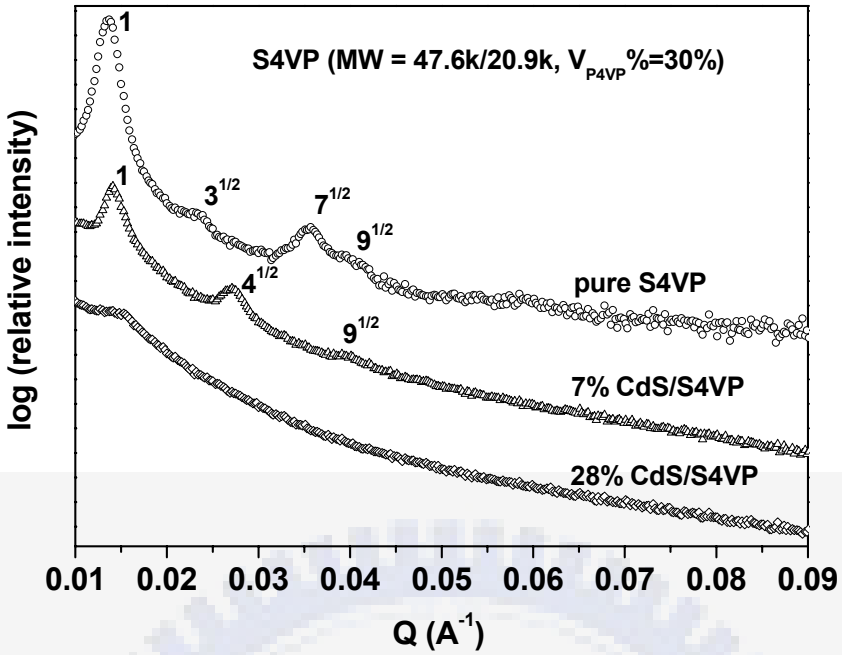
S4VP (MW = 47.6k/20.9k, V$_{P4VP}$%=30%)
1
1
3$^{1/2}$
7$^{1/2}$
9$^{1/2}$
4$^{1/2}$
9$^{1/2}$
pure S4VP
7% CdS/S4VP
28% CdS/S4VP
log (relative intensity)
0.01
0.02
0.03
0.04
0.05
0.06
0.07
0.08
0.09
Q (A^{-1})

Figure 4-2

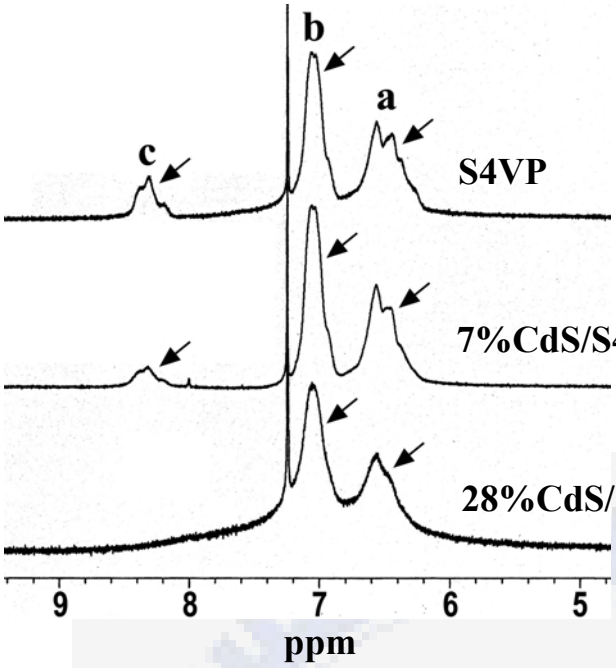
b
a
c
S4VP
7%CdS/S4VP
28%CdS/S4VP
9
8
7
6
5
ppm

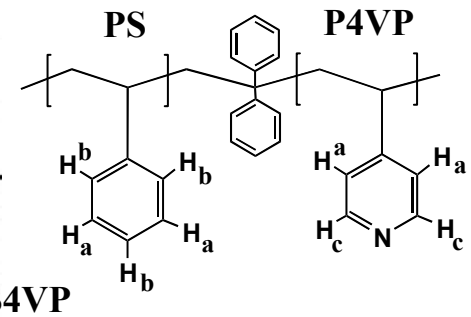
PS
P4VP
H^b
H_b
H_a
H_a
H_b
H^a
H_a
H_c
N
H_c

Figure 4-3

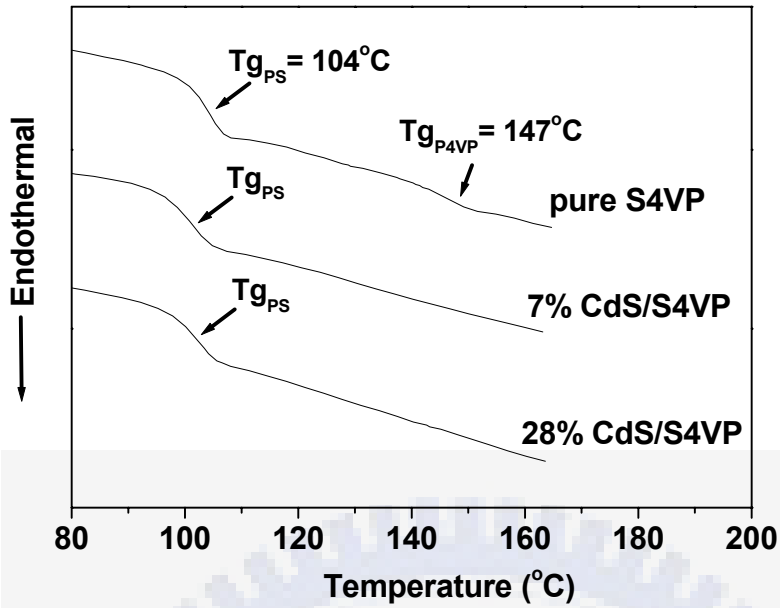
Tg$_{PS}$= 104°C
Tg$_{P4VP}$= 147°C
pure S4VP
Tg$_{PS}$
7% CdS/S4VP
Tg$_{PS}$
28% CdS/S4VP
Endothermal
80
100
120
140
160
180
200
Temperature (°C)

Figure 4-4

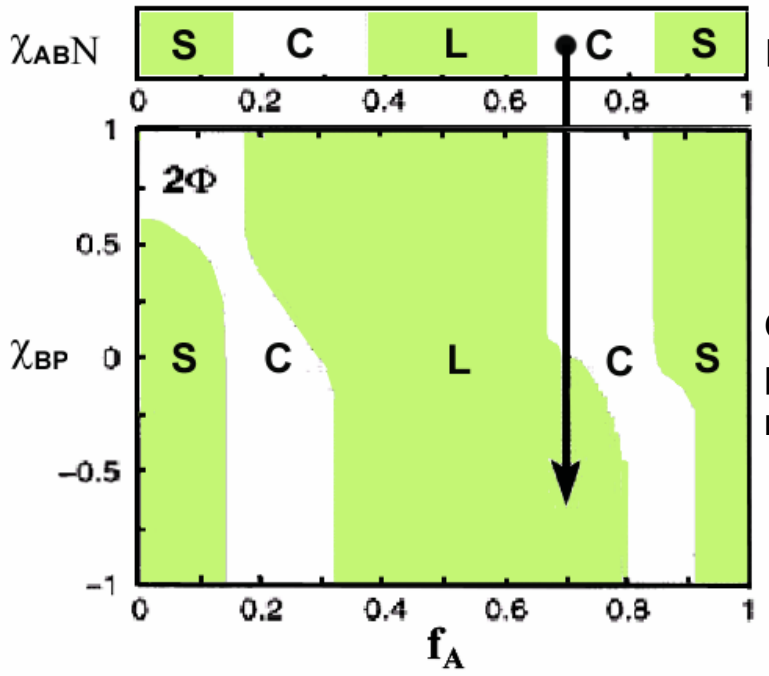

pure S4VP

CdS/S4VP particle/block copolymer mixture system

Figure 4-5

Chapter 5: Conclusions

In the bulk CdS/SEO system, surface-modified CdS nanoparticles selectively dispersed in a PEO block hinder crystallization of PEO and maintain their original optical properties in both cases of CdS/HSEO and LSEO bulk samples. Moreover, the CdS-infiltrated PEO domains, in the case of CdS/HSEO, are transformed from originally hexagonally-packed cylindrical structures to BCC or SC structures because of the inhibition of the crystallization in PEO and minimization of the surface energy of CdS/PEO domains. In the case of bulk CdS/LSEO, however, segregation of CdS nanoparticles results in an increase in the inter-cylinder distance of the HEX CdS/LSEO, but the ordered nanostructure of LSEO is destroyed by high CdS content. We can conclude that CdS nanoparticles hinder crystallization of PEO domains, and induce the composites form a structure decided by the volume fraction only. (**BCC** structure for $\mathbf{V_{PEO/HSEO} = 0.11}$**, and HEX structure for** $\mathbf{V_{PEO/LSEO} = 0.39}$), in the **Amorphous-Crystalline Bulk SEO** system,

Moreover, we have provided a method to control the spatial position of pre-synthesized CdS nanoclusters using a specific interaction between surface ligands and one block of a self-assembled diblock copolymer template by first selectively dispersing these nanoparticles in one particular block of a diblock copolymer, in bulk, and then using solvent selectivity to sequester CdS nanoparticles in the block copolymer thin film. The inter-domain distance of the nanoclusters can be altered by changing the molecular weight of the other block of the diblock copolymer. Long-range order in CdS/LSEO thin films has been obtained using a patterned substrate. The incorporated nanoparticles retain their luminescence characteristics, as in the pure state. The CdS nanoparticles can be replaced by

other nanoparticles or quantum dots, as long as proper surface ligands can be found.

In the case of CdS/LSEO thin films, the morphological transformation from PEO cylinders to spheres in thin films, due to the incorporation of CdS nanoparticles, is clearly observed in AFM, TEM and SEM images. The transformation is explained by hydrogen bonding interactions between surface-hydroxylated CdS and PEO, as demonstrated by NMR studies. Hydrogen bonding changes the chemical environment of PEO next to the CdS clusters. In the case of 28 %wt CdS/SEO thin films, the ordered arrangement of CdS clusters is fabricated via an SEO block copolymer template.

In the case of CdS/S4VP system, CdS nanoparticles segregated P4VP domains of S4VP block copolymers by the hydrogen bonds induces the morphological change from hexagonally-packed P4VP cylinders to lamellar structure of CdS/S4VP composites. The experimental data of the morphological transformation of CdS/S4VP composites is consistent with the prediction of the nanoparticles/block copolymers system in theory.

Publication Lists

Siao-Wei Yeh, Kung-Hwa Wei, Ya-Sen Sun, U-Ser Jeng, Keng S. Liang, "Morphological Transformation of PS-b-PEO diblock copolymer by Selectively Dispersed Colloidal CdS Quantum Dots", *Macromolecules* **2003**, *36*, 7903.

U-Ser Jeng, Ya-Sen Sun, Hsin-Yi Lee, Chia-Hung Hsu, and Keng S. Liang, **Siao-Wei Yeh**, Kung-Hwa Wei, "The binding effect of surface-modified cadmium sulfide on the microstructure of PS-b-PEO block copolymers", *Macromolecules* **2004**, *37*, 4617.

Siao-Wei Yeh, Yao-Te Chang, Chia-Hung Chou and Kung-Hwa Wei, "Effect of Surface-Hydroxylated CdS Nanoparticles on the Morphological Transformation of Poly(styrene-b-ethylene oxide) Thin Films", *Macromolecular Rapid Communications* **2004**, *25*, 1679.

Siao-Wei Yeh, Tzung-Luen Wu, Kung-Hwa Wei, Ya-Sen Sun, and Keng S. Liang, "Effect of Incorporated CdS Nanoparticles on the Crystallinity and Morphology of Poly(styrene-b-ethylene oxide) Diblock Copolymer", *J. Polym. Sci. B Polym. Phys.* **2005**, accepted.

Siao-Wei Yeh, Tsung-Lun Wu and Kung-Hwa Wei, "Spatial Position Control of Pre-synthesized CdS Nanoclusters using a Self-assembled Diblock Copolymer Template", *Nanotechnology* 2004, revised.

Siao-Wei Yeh, Yao-Te Chang, Chia-Hung Chou, Kung-Hwa Wei, Ya-Sen Sun, and Keng S. Liang, "CdS Nanoparticles Induce a Morphological Transformation of Poly(styrene-*b*-4-vinylpyridine) from Hexangonally-packed Packed Cylinders to a Lamellar Structure", *Macromolecules* **2004**, submitted.

學經歷資料

- 姓名：葉孝蔚
- 性別：男
- 生日：66 年 10 月 30 日
- E-mail address：bluebird.mse88g@nctu.edu.tw
- Tel：(學校) 03-5731771 (手機) 0937-642882
- 聯絡地址：新竹市 300 大學路 1001 號
  國立交通大學材料與工程研究所

學歷

博士候選人：國立交通大學材料科學與工程研究所　1999. 9 ~ present
大學：國立交通大學應用化學系　1995. 9 ~ 1999. 6

參與計畫

- 量子點/自身組織塊式高分子奈米複合材料。
- 化學機械研磨墊(CMP Pad)之無機層狀材/聚胺基甲酸酯(PU)發泡體奈米複材研究。
- 低介電溶膠凝膠聚亞醯胺(PI)奈米複合材料之製備。
- ITO 導電玻璃製備與分析。

專長

- 奈米操控與分散技術：
  1. 奈米模板(nano-template or nano-mask)之塊式高分子薄膜操控與分析。
  2. 無機量子點奈米粒子之合成、特性、界面改質分散技術與結構鑑定分析。
  3. 排列無機奈米粒子形成各種奈米結構之操控技術。
  4. 低介電聚亞醯(PI)與胺聚胺基甲酸酯(PU)發泡體/無機物混成材之特性。
- 化學機械研磨墊(CMP Pad)之研究。
- ITO 導電玻璃製備與分析。

專業儀器操作

原子力顯微鏡 (AFM)、穿透式電子顯微鏡 (TEM)、掃瞄式電子顯微鏡 (SEM)、X 光繞射分析、超薄切片機、光學量測儀器、電性量測分析、紅外線光譜分析、紫外光-可見光光譜分析、熱分析(DSC, TGA, TMA)、粒徑分析、及真空蒸鍍設備操作。